Universität Zürich[UZH]

Geographisches Institut

Soil properties and erosion rates of treethrows on the Upper Peninsula of Michigan, USA

GEO 511 Master's Thesis

Author: Annika Spaar, 20-716-635

Supervised by: Prof. Dr. Markus Egli, Dr. Pavel Samonil (samonil@vukoz.cz)

Faculty representative: Prof. Dr. Markus Egli

24.04.2026

Abstract

Tree uprooting (treethrow) is a major mechanical disturbance in forest ecosystems and creates a characteristic pit-and-mound microtopography that influences soil development, sediment redistribution, and erosion over long timescales. This study investigates how mechanical disturbance affects soil properties, soil development, and short- and long-term erosion rates in sandy Albic Podzols on the Upper Peninsula of Michigan, USA. Two treethrow sites of different age were examined, a young treethrow dated to around 1840 CE and an old treethrow dated to approximately 4'077 BCE, each compared with their nearby undisturbed control site.

Field observations, soil profile descriptions, pH, bulk density, elemental analysis, and portable optically stimulated luminescence (pOSL) were combined with fallout plutonium ($^{239+240}$Pu), meteoric ^{10}Be, and in situ ^{10}Be to assess disturbance patterns and erosion rates across different timescales. The results show that treethrow events significantly alter the morphology and horizonation of soil profiles. The young mound exhibits a simplified and disturbed soil profile, whereas the old mound shows clearer horizon differentiation and greater pedogenic recovery. Erosion estimates vary depending on the tracer and timescale, but overall, disturbed sites differ from undisturbed soils in both erosion behaviour and soil development.

The study demonstrates that treethrow is not only a short-term ecological disturbance, but also a long-term pedological and geomorphological process that contributes significantly to soil heterogeneity and landscape evolution in temperate forest environments.

Acknowledgements

I would like to thank my supervisor Prof. Dr. Markus Egli for supporting me throughout the thesis work. Furthermore, I would like to thank Dr. Pavel Šamonil and his research group for giving me the opportunity to join their field trip to the Upper Peninsula of Michigan. My thanks also go to Prof. Dr. Randall J. Schaetzl for joining and supporting us during the field trip. My gratitude goes to the Geographie Alumni UZH for financially supporting my field trip to Michigan. Finally, I also thank my friends and family for supporting me during the thesis.

Table of Contents

List of Figures

List of Tables

1 Introduction

Tree uprooting (treethrow) is a common mechanical disturbance in forest ecosystems often occurring as a result of natural hazards, such as wind or snowstorms (Hellmer et al., 2015). Mechanical disturbances include natural processes such as wind, oversaturation of sediments and loading of snow and ice. The process of treethrow is often explained as a process driven by strong winds. This mechanical disturbance can exceed the mechanical stability of the root-soil system, leading to effects such as displacement of root material, soil, loose sediment and fractured bedrock (Hellmer et al., 2015). Treethrow occurs when sediment and bedrock, which are attached to the roots, get uplifted when a tree falls. This process leads to vertical and horizontal displacement of soil (and roots) (Schaetzl et al., 1990).

Since a part of the soil is excavated, a hole, called a pit is created. The root plate, which held the roots, sediments and organic matter together, starts to fall apart when the roots decay. The accumulation of this released material from the root plate, starts to form a mound, a small hill. The area affected by such treethrow and creating such a landscape is called a pit and mound microtopography (Šamonil et al., 2016; Schaetzl et al., 1990). Because the material from the root plate should accumulate below it, forming a mound, the volume and composition of these two structures should be the same. However, the slopes created by these pit and mound topographies mean that the excavated material can fall back into the pit. This leads to a volume difference between the root plate and the mound.

When wind throw occurs, trees fall in the wind direction. Uprooting of trees exposes bare soil to the atmosphere, making it more susceptible to erosion through rainfall, surface runoff, wind and gravity. The degree of soil development is reduced immediately after the uprooting event (Šamonil et al., 2016). This is mainly due to the disruption of the horizons, where the soil horizons get mixed. Topsoil consisting of humus gets mixed with deeper mineral-horizons. This can destroy and influence the stability of the soil. The soil is less developed and less stable after an uprooting event, which makes the soil more affected by erosion (Schaetzl et al., 1990). Erosion rates peak directly after the event occurred, due to exposure of the soil and the formed pit and mounds. It can stabilize over time through regrowing vegetation, which stabilizes the soil and keeps it from eroding. Disturbed sites experience more erosion in comparison to undisturbed sites. The difference is especially high directly after the event. Although it stabilizes over time, there is still overall more sediment redistribution in the disturbed area than the undisturbed site (Hellmer et al., 2015).

In the study area on Michigan's Upper Peninsula, treethrow is the primary disturbance process affecting sandy Albic Podzols that developed on glacial outwash deposits (Šamonil et al., 2016). These coarse-textured soils favour the long-term preservation of pit-and-mound microtopography, which can persist for more than 6'000 years (Šamonil et al., 2013). As a result, treethrow events influence ecosystem dynamics, soil formation and erosion and shape the geomorphology of the affected sites, making this area particularly suitable for investigating the influence of uprooting on soils (Šamonil et al., 2013).

Despite the recognised importance of treethrow disturbances for soil redistribution and landscape evolution, quantitative estimates of erosion associated with these microtopographic features remain limited. To address this knowledge gap, this study investigates soil erosion, sediment redistribution and their influence on soil properties in the Upper Peninsula of Michigan, at sites that are affected by treethrow disturbances. Sites representing different stages of disturbance are compared, including a recent treethrow created around 1840 CE, an older treethrow created around 4’077 BCE, and undisturbed control sites for each treethrow.

Erosion rates are estimated using plutonium ($^{239+240}Pu$) isotopes from radioactive fallout and meteoric and in situ ^{10}Be. Additionally, portable Optically Stimulated Luminescence (pOSL) is applied to determine if sediment disturbance associated with tree uprooting events occurred. Soil properties are analysed through the horizon, pH and Feo/Alo concentrations. By combining these methods, the study aims to improve the understanding of how treethrow-induced microtopography influences soil erosion, sediment redistribution and soil properties in sandy temperate forest soils.

1.1 Previous Studies & State of the Art

Already in the 19th century tree uprooting events were described. Shaler (1891) described that when a forest is overturned by a strong wind, trees are being uprooted. The uprooted mass has often a diameter of up to 3 meters and contains a cubic meter or more of soil. The pit can be several decimetres deep. The pit starts refilling with plants while the roots decay and the soil falls back on the ground over a layer of humus. The decay of roots can leave canals, that are later filled with material falling from the surface or from the side walls (Shaler, 1891). Holmes (1893, cited in Lutz and Griswold, 1939) already described the surface as that it was varied by countless humps and hollows and that the observed site was uprooted by a tornado. Furthermore, the entire mass of soil to a depth of several meters has been uprooted. Van Hise (1904, cited in Lutz and Griswold, 1939) noted that this process is well illustrated in the Lake Superior region (Lutz and Griswold, 1939). Lutz and Griswold (1939) conclude, that tree roots play a significant role in modifying soil morphology. Disturbances caused by roots can take various forms: the uplift and displacement of large soil masses when trees are uprooted, the formation of channels that remain after roots decay and are later filled with material from the surface or surrounding soil, the lateral displacement of soil caused by root growth, and soil movement induced by tree moving from side to side during strong winds. The authors argue that many morphological features of soil profiles previously attributed to frost heave in periglacial climates may also be explained by the influence of tree roots. They emphasize that the role of roots in shaping soil morphology is often underestimated and that all forest soils have been disturbed to some extent by tree roots (Lutz and Griswold, 1939). One of the earliest mentions of the term treethrow was already in 1954 by Goodlett (1954, cited in Small, 1997). Previous work on treethrow erosion has shown that mound evolution is dominated by progressive root plate disintegration and connected surface erosion. Over a 45-year period the volumetric changes of a mound in Pennsylvania were documented, showing that erosion rates are higher right after the event in 1950 and much lower at the end of the time period 1995. These results were one of the first quantitative studies about erosion at treethrows and it was achieved by historical photo comparison and volumetric mound measurements (Small, 1997).

Many more studies about treethrow and the effects were researched and published by Schaetzl and Šamonil, with which I had the opportunity to join the research group on the field trip to Michigan.

Multiple studies about the uprooting of trees (treethrow) have been conducted on Podzols in northern hardwood forests in the region of the Great Lakes in the USA. Some additional studies were performed in Europe, Russia and New Zealand, which can be seen in Figure 1 below (Šamonil et al., 2010).

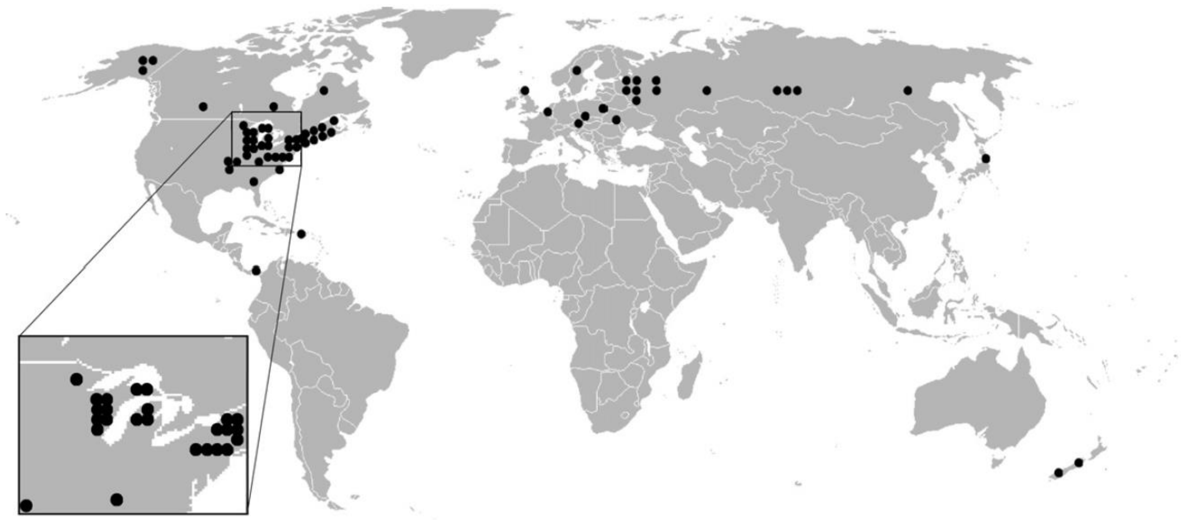

Figure 1: Overview of treethrow-related studies conducted around the world (up to the year 2010). Source: Šamonil et al. (2010).

Building on these early observations and later studies, research on treethrow processes in the Upper Peninsula has increasingly focused on their geomorphological and pedogenic significance. Treethrow is the most obvious and significant biogeomorphological disturbance factor in many forest soils (Šamonil et al., 2018). Modern studies examine treethrow not only as a disturbance event but also as a long-term driver of soil development, erosion dynamics, and landscape heterogeneity in forest ecosystems (Šamonil et al., 2010, 2018; Schaetzl, 1990).

Treethrows, the pits and mounds formed by uprooted trees, are understood as long-lasting biomechanical disturbances that shape soil properties, erosion processes, and pedogenesis in forest landscapes. As shown in Šamonil et al. (2010), research has focused on ecological conditions in pit-mound microsites, the area of pit-mounds in different landscapes, the age of pit-mounds, the rotation period and the effect of tree uprooting on soil properties. Šamonil et al. (2010), conclude that pit-mound microtopography creates distinct ecological microsites, that differ in moisture, temperature and organic matter dynamics. Furthermore, treethrow can influence large portions of forest landscapes and uprooting has measurable long-term effects on soil morphology and chemistry. Therefore, treethrow represents a fundamental soil-forming and soil-mixing process in temperate forests (Šamonil et al., 2010). In sandy, podzolized environments like the Upper Peninsula, treethrow microtopography can persist for centuries, and under favourable conditions, even millennia (Šamonil et al., 2010), especially where soils are coarse, litter cover is continuous, and freeze-thaw processes reduce surface erosion. Local soil texture and climate strongly control the persistence and pedogenic expression of treethrow features. Coarse-textured soil and cool, humid conditions favour long-term preservation of the microrelief. They therefore have a lasting impact on soil formation processes in temperate forests (Schaetzl, 1990; Schaetzl et al., 1990; Schaetzl and Follmer, 1990). Mechanically disturbed soils in pits show increased moisture retention and organic enrichment, which promotes leaching and accelerated profile differentiation compared to undisturbed soil. In contrast to that, mounds, which mainly consist of mixed subsoil and root plate material, generally remain less developed and more susceptible to erosion and surface transport (Schaetzl, 1990). Comparisons between disturbed (pit-mound) and undisturbed sites show, that disturbances generally accelerate early pedogenesis in pits compared to undisturbed control areas, while mounds can remain pedogenetically undeveloped over longer periods of time, leading to greater soil heterogeneity in disturbed landscapes. In this divergent soil formation processes, pits often exhibit deeper horizon development than the surrounding soil, while mounds lag in soil development (Šamonil et al., 2010, 2018; Schaetzl, 1990). Mechanical soil disturbance events initially increase surface instability and erosion rates, compared to undisturbed forest areas. Over longer timescales, frequently disturbed microtopography, leads to a mosaic of soil development stages in the affected area, which differ significantly from undisturbed soils. These microtopographies show a higher spatial variability in terms of soil chemistry, soil structure and hydrology (Šamonil et al., 2018; Schaetzl, 1990).

While many of these studies discuss mound degradation and persistence, they rarely directly quantify erosion rates of treethrows, especially mounds, in Michigan.

1.2 Formation of mounds and treethrows

When a large tree gets uprooted, the root plate pulls out a lens of soil and creates an irregularly shaped hole, a pit. The soil within the lens gradually loosens from the roots and settles beside the pit, forming an uneven mound, with parts of it breaking away and falling back into the pit. Through these processes the typical pit-mound topography is created (see *Figure 2*) (Šamonil et al., 2015), which covers around 16.9% of the surface in the study area (Šamonil et al., 2013). Figure 2 shows this process, from the standing over uprooted tree with the root plate and the resulting pair of pit and mound.

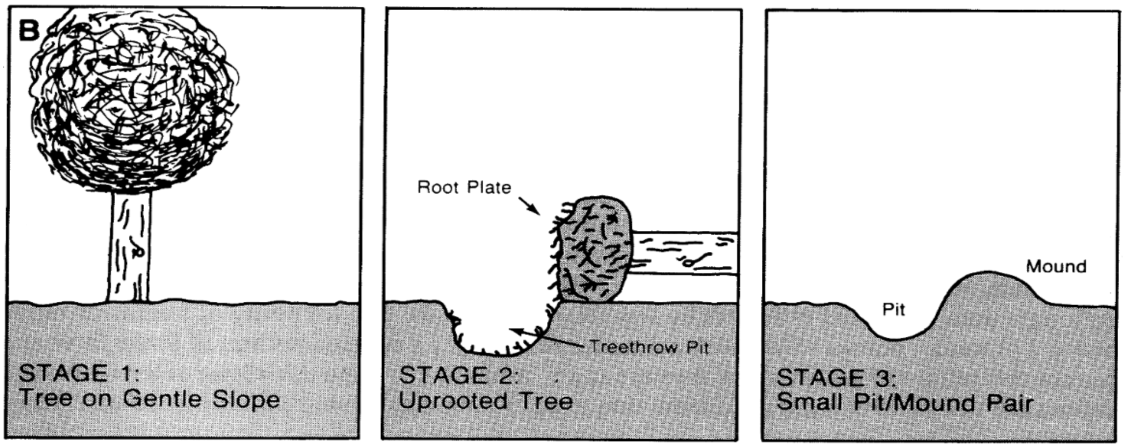

Figure 2: Schematic figure of the development of pit and mound pairs. Source: Schaetzl and Follmer (1990).

Tree uprooting can be understood as the fall of a tree during which the root plate is torn from the soil, regardless of the specific cause, such as wind, snow, ice or competition (Šamonil et al., 2010). As a form of macroturbation, treethrow results in the vertical displacement and lateral redistribution of soil (Šamonil et al., 2010; Schaetzl et al., 1989; Tejnecký et al., 2015).

Tree uprooting disrupts the usually slow and progressive development of soils, which typically involves mineral weathering, decomposition of organic matter, and the vertical redistribution of these products into different horizons, forming organized soil profiles. Treethrow represents a regressive process because it interrupts and resets this pedogenic progression. By mixing materials that were originally systematically stratified, tree uprooting affects soil horizonation. After the tree has fallen, the re-establishment of horizon development and profile differentiation is strongly influenced by the microtopography created by the disturbance. The resulting pits tend to accumulate additional washed-in litter and mineral material and receive increased percolating water, conditions that generally facilitate horizon development and translocation. In contrast, mound soils experience reduced leaching, greater drying, enhanced surface runoff, and potentially accelerated erosion (Šamonil et al., 2015). Over time the soil surface gradually evens out, the mound gets smaller and the pit fills up. Figure 3 shows how the pit fills up over time and the mound degrades over time until both features are evened out again. Both showing new horizon sequences.

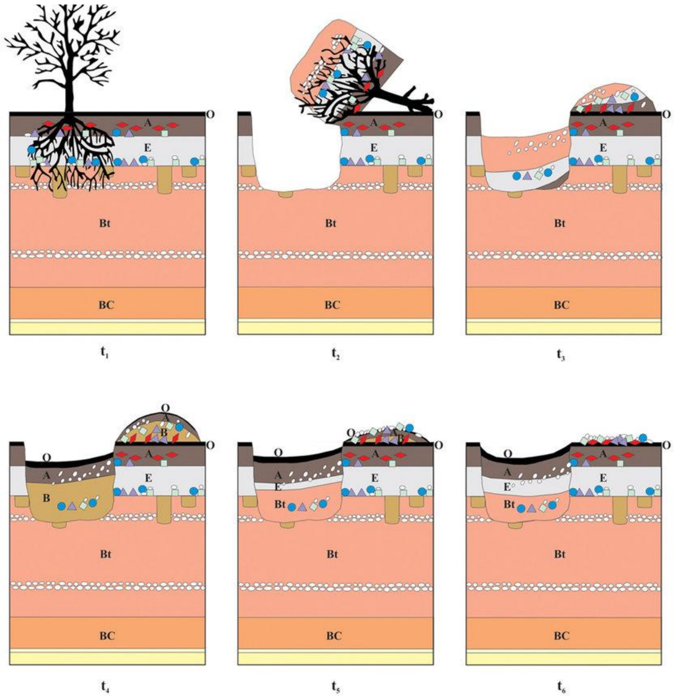

Figure 3: Timeline of soil development after a treethrow. Source: Gruškovnjak (2020).

The pit-mound structures create microtopography with microclimate conditions within pits and mounds. Over time the created microtopography influences erosion, water movement and soil formation. Thus, treethrows actively shape the landscape and affect soil processes for hundreds or even thousands of years (Šamonil et al., 2010; Tejnecký et al., 2015). The oldest treethrow with an age of 6’183 years, was found in the stable landscape on the Upper Peninsula (Šamonil et al., 2018). The study area contains sandy, porous soils that minimize runoff, a continuous layer of forest litter and vegetation cover, surface concentrations of gravel which can act as an armor, features have a large initial size and soil freezing occurs. All these factors might be a reason for the longevity of treethrow mounds in these regions (Schaetzl and Follmer, 1990).

1.2.1 Pit and mound features

The chemistry of the soil develops differently in pit, mounds and the surrounding soil (Šamonil et al., 2018). In the following Table 1 key differences between pit and mounds are listed (Šamonil et al., 2018).

Table 1: Properties and processes of pit and mound features (Šamonil et al., 2020, 2018, 2015)

Process	**Pit**	**Mound**
Starting process	Sink with material accumulation	Discharge with organic and mineral material
Soil origin	Filled with surface material -> acidic	From subsoil -> less acidic
Water dynamics	Humid, water accumulates	Drier, better drained
pH-value	Lower (more acidic) due to organic accumulation	Slightly higher pH than in the pit (less organic input)
Nutrient availability	Initially higher, later heavy losses due to leaching	Lower nutrient losses
Podzolization	Fast (forms Bhs, E horizons)	Slow or delayed
Dominant process	Eluviation & leaching	Slow development, often backshifting
Erosion	Chemical erosion (nutrient loss)	Mechanical erosion by rain & wind

Pedogenetic processes in mounds tend to regress or rejuvenate over longer periods of time. Although the mound is disturbed after an uprooting event, soil-forming properties that resemble the original soil profile over the course of decades to centuries through weathering, rooting, biological activity and organic matter can re-establish. In this backshifting process, humus builds up, the pH value drops, nutrients are redistributed, and a new A horizon forms. Through these processes soil properties return to the initial conditions, therefore it is a regression towards the undisturbed state (Šamonil et al., 2018, 2015; Schaetzl, 1990). Figure 4 shows the processes which happen after a mechanical disturbance in pit and mounds.

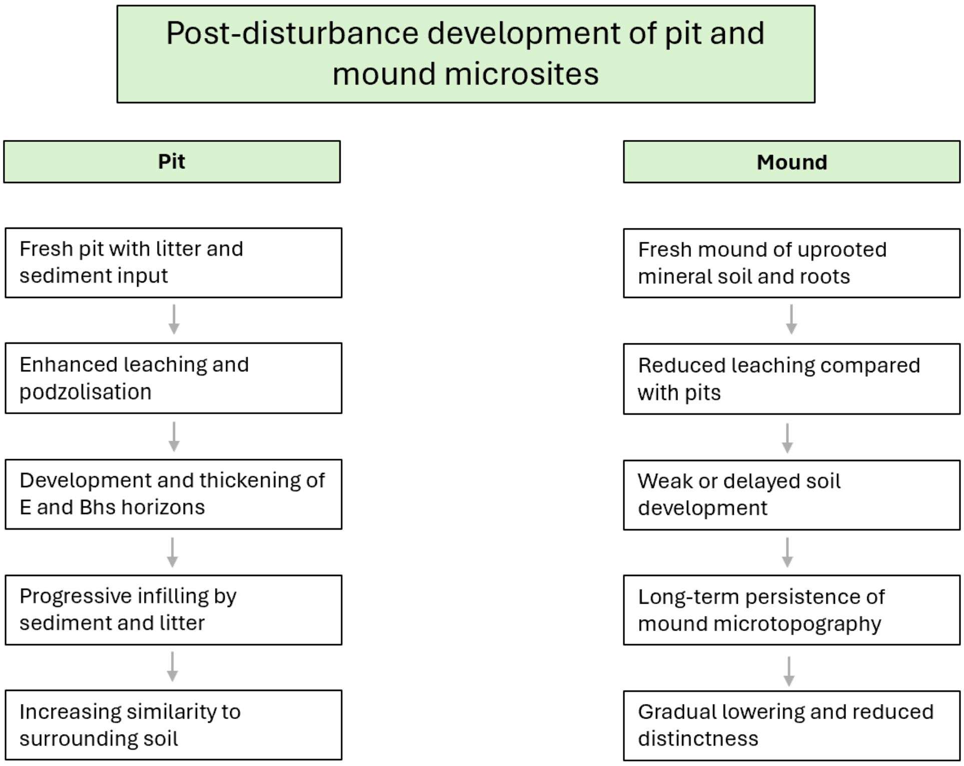

Figure 4: Post-disturbance development of pit and mound microsites after a treethrow. Figure was created in PowerPoint (based on Nelson et al., 2021; Šamonil et al., 2018).

1.3 Theoretical Background of the Methods

This section presents the theoretical basis of the methods used, to show why they are suitable.

1.3.1 Portable Optically Stimulated Luminescence (pOSL)

Portable Optically Stimulated Luminescence (pOSL) shows when minerals (quartz and feldspar) were last exposed to sunlight. The signal of OSL (quartz) gets bleached fast through sunlight, while the IRSL (feldspar) signal is bleached slower and by infrared light. With this method it is possible to determine the last time the specific soil layers were exposed to sunlight at the surface. However, in contrast to laboratory OSL dating, portable OSL measurements provide relative luminescence signal intensities and do not calculate absolute ages (Muñoz-Salinas et al., 2011; Sanderson and Murphy, 2010).

Minerals store energy from ionising radiation over time. Quartz (SiO_2) and feldspar can accumulate electrons which are generated because the minerals are constantly exposed to natural radioactivity in the surrounding soil. The longer the mineral remains buried in the dark, the more electrons accumulate in these crystal lattices (Muñoz-Salinas et al., 2011). If the minerals come into contact with sunlight again, the luminescence signal is reset to 0. Sunlight, especially blue and infrared light, has enough energy to release the trapped electrons. The electrons return to their original positions, emitting light (luminescence) in the process. The longer the layers are exposed to the sun, the more the signal is reduced (bleached). After sedimentation the process starts again. The longer the soil layer was buried, the stronger the detectable luminescence signal (Rhodes, 2011). The measured signal intensity reflects the relative amount of accumulated radiation and therefore allows comparison of burial duration between the different soil layers (Sanderson and Murphy, 2010). This makes it possible to detect disturbed and undisturbed soil layers.

1.3.2 Elemental Analysis (EA)

The elemental analysis of soil for total carbon (C) and nitrogen (N) is based on the complete oxidation of C- and N-containing compounds to CO_2 and N_2 during high-temperature combustion. In quantitative combustion, the quantities of these gases are directly proportional to the total C and N content and can be measured by thermal conductivity detection (Muccio and Jackson, 2009). In the analysis of stable isotope ratios, the same gases produced are used to determine the relative abundances of $^{13}C/^{12}C$ and $^{15}N/^{14}N$ using isotope ratio mass spectrometry (IRMS), in which ions are separated. The isotopic compositions are expressed as $\delta^{13}C$ and $\delta^{15}N$ values (Muccio and Jackson, 2009).

Fluctuations in $\delta^{13}C$ and $\delta^{15}N$ reflect isotopic fractionation during biological and biogeochemical processes such as organic matter decomposition, mineralisation, nitrification and denitrification. In addition, total carbon content can serve as an indicator of soil erosion, as the preferential removal of organic-rich topsoil typically leads to a reduction in carbon concentrations in eroded areas (Holz and Augustin, 2021).

1.3.3 Meteoric ^{10}Beryllium

Meteoric ^{10}Be is a cosmogenic radionuclide that is produced in the atmosphere by spallation of oxygen and nitrogen and subsequently reaches the Earth's surface through deposition. Meteoric ^{10}Be accumulates continuously on the soil surface (Clow et al., 2020; Jelinski et al., 2019). After deposition, meteoric ^{10}Be is adsorbed onto fine-grained soil particles (clay-minerals such as iron and aluminium oxides) and accumulates in the near-surface regolith. Its inventory reflects the balance between atmospheric input, radioactive decay, vertical translocation and physical removal through erosion (Clow et al., 2020). Under stable conditions, the concentration or inventory of meteoric ^{10}Be in soil can therefore be related to long-term mass loss rates. Higher erosion rates shorten the residence time of soil particles and limit the accumulation of ^{10}Be, while lower erosion rates allow for greater accumulation. Therefore the more ^{10}Be is found in the soil, the longer the surface was exposed and the lower the erosion (Jelinski et al., 2019). ^{10}Be accumulates in the top layer of the soil and the concentration decreases with depth, due to atmospheric deposition at the surface and limited downward migration (Jelinski et al., 2019). By measuring the ^{10}Be concentrations in different soil depths, it is possible to see if the soil was disturbed or undisturbed (Clow et al., 2020; Jelinski et al., 2019). A different distribution than a decline of ^{10}Be with depth, indicates soil mixing, erosion or deposition (Jelinski et al., 2019). By incorporating independently constrained delivery fluxes and the known half-life of over one million years, meteoric ^{10}Be provides a robust tracer for estimating soil redistribution and erosion rates over timescales ranging from hundreds to thousands of years (Clow et al., 2020; Jelinski et al., 2019).

1.3.4 In situ ^{10}Beryllium

In situ ^{10}Be is a cosmogenic radionuclide formed directly within the mineral-usually quartz-through interactions with secondary cosmic radiation when rock or soil is exposed near the Earth's surface (Gosse and Phillips, 2001; Lal, 1991). Unlike meteoric ^{10}Be, it does not originate from atmospheric deposition but is produced directly within the material itself (Gosse and Phillips, 2001). The concentration of in situ ^{10}Be depends on the duration of surface exposure and the rate of weathering: during long, undisturbed exposure, more ^{10}Be can accumulate, whilst rapid erosion or weathering reduces the accumulation (Gosse and Phillips, 2001; Lal, 1991). As the production rate decreases exponentially with depth due to shielding by the overlying material, undisturbed soil or regolith profiles typically show the highest concentrations near the surface and decreasing values with depth. Deviations from this pattern may indicate soil mixing, erosion or sediment accumulation (Fülöp et al., 2015). In situ ^{10}Be is therefore used for quantifying long-term denudation and soil transport rates over periods ranging from several thousand to hundreds of thousands of years (Gosse and Phillips, 2001).

1.3.5 Plutonium

Plutonium (Pu) isotopes, particularly ^{239}Pu and ^{240}Pu, are anthropogenic radionuclides. The method is based on the determination of ^{239}Pu + ^{240}Pu to investigate soil erosion rates and the stability of soil profiles. It relies on plutonium isotopes that were released into the atmosphere during atmospheric nuclear weapon tests, which were conducted between 1945 and 1980, with peak fallout in the 1950s and 1960s and were distributed approximately evenly around the globe (Dowell et al., 2023; Xu et al., 2015). After deposition, plutonium adsorbs to fine soil particles, especially clay minerals and organic matter, which leads to accumulations in the upper soil horizons under undisturbed conditions (Dowell et al., 2023). Due to its high particle reactivity and low solubility, plutonium has very limited vertical mobility in soil. Significant downward redistribution usually only occurs as a result of physical disturbance processes, such as macroturbation, uprooting or erosion (Alewell et al., 2017; Dowell et al., 2023). This makes it usable as a tracer of soil movement. To quantify if erosion or deposition occurs, Pu activities measured in the different soil profiles are compared to a reference site, where the inventory represents the original atmospheric fallout (in this case from 1963). By comparing the cumulative Pu activity of each sampling site with the reference site's Pu inventory, it is possible to estimate if soil material within the profile was removed through erosion or accumulated through sediment deposition (Xu et al., 2015). Under undisturbed conditions, the biggest part of fallout plutonium is concentrated in the topsoil and a well-defined depth distribution in the profile is expected. Variations from this pattern, indicate post-fallout soil redistribution (Meusburger et al., 2016; Schimmack et al., 2001). However, this method only provides relatively short-term erosion rates (Dowell et al., 2023).

1.4 Research Question and Hypotheses

The aim of this study is to determine how mechanical disturbances, especially treethrows, influence the soil and landscape in the Upper Peninsula in Michigan, USA. The focus is on determining short- and long-term erosion rates of mounds of selected treethrows and comparing them with undisturbed sites and between young and old mounds. By quantitatively determining the erosion rates of mounds, this study aims to fill the research gap of limited quantitative erosion data on treethrows and gain a better understanding of erosion connected to mechanical disturbances in the Upper Peninsula. The research addresses the following questions:

"How do mechanical disturbances influence soil properties, erosion, and soil development in sandy Albic Podzols of the Upper Peninsula in Michigan?"

"How do erosion rates and the degree of soil development vary between disturbed sites and undisturbed sites in the short and long term?"

Based on the current knowledge, the following working hypotheses were formulated:

H1: Disturbed sites show weaker horizon differentiation than undisturbed sites.

H2: Old treethrows align more with the undisturbed state than profiles of young treethrows.

H3: Disturbed soils have a higher erosion rate compared to undisturbed soils.

H4: Disturbed and undisturbed soils will have a similar erosion rate in the long-term.

I expect disturbed soils to have a higher erosion rate in the short-term, due to factors such as loss of vegetation and soil exposure to the air. Steep mound walls might be created as well during such uprooting events, which can increase the erosion rate. Over time, disturbed soils can recover and stabilize, including vegetation, which has a stabilizing function on soils. This will probably lead to less erosion than right after the event and to a similar amount of erosion as the undisturbed soils have. To test these hypotheses, old and young mounds are sampled. By answering these questions, the study aims to improve the understanding of effects on erosion by mechanical disturbances in forests. The results will provide insights into the erosion behaviour of soils in the Upper Peninsula in areas where treethrow occurs and may support the management of managed forests.

2 Study Area

The study area is located on the Upper Peninsula near the town of Strongs in Michigan in the United States (see Figure 5 and Figure 6 below). Figure 5 shows the two chosen treethrows, treethrow 2 and treethrow 3. Since this work is part of a larger study on treethrows in the Upper Peninsula, for which several papers have already been published, the same study area was chosen again (Šamonil et al., 2016). The soils of the study area evolved on glacial outwash deposits and contain a high proportion of sand. They are classified as Albic Podzols. The study area extends over an elevation gradient of 215-270 metres (Šamonil et al., 2013). The forest is a mix of northern deciduous trees, where maples dominate. The forest was previously managed. The prevailing climate is cool and humid with persistently low soil temperatures (Šamonil et al., 2016). The sample sites were chosen to represent a young and an old treethrow in the study area.

Figure 5: The map shows the 2 selected treethrows near Strongs in the Upper Peninsula, Michigan. The map was created in QGIS. The sites are only about 36 m apart. The "Point Displacement" function was used on the map to make both points visible and prevent them from overlapping.

Figure 6: Location of the selected study area on the Upper Peninsula in Michigan, USA. Created in QGIS.

2.1 Background Information on Study Area

The study area is a sandy, well-drained, low-relief upland. It lies in a mature deciduous-coniferous forest near the small town of Strongs (Schaetzl et al., 2020), in the eastern Upper Peninsula Lowlands of Michigan, shown in Figure 7 (Schaetzl et al., 2013). Locally the site is known as Hulbert Island, see Figure 8 (Schaetzl et al., 2013), as it is located within the former glacial Lake Algonquin (Schaetzl et al., 2020). The area is mostly a dry upland with a few kettle lakes. The area is wetter in the south-eastern part of the region, where the sample sites are located. The terrain has a low elevation and low relief landscapes which was variously shaped by glacial deposition and meltwater and subsequently influenced by post-glacial lakes (lacustrine) and wind-driven (aeolian) processes (Schaetzl et al., 2013).

Figure 7: Physiographic regions of Michigan, showing the Eastern Upper Peninsula Lowlands, Source: Schaetzl et al., 2013, Fig. 1.

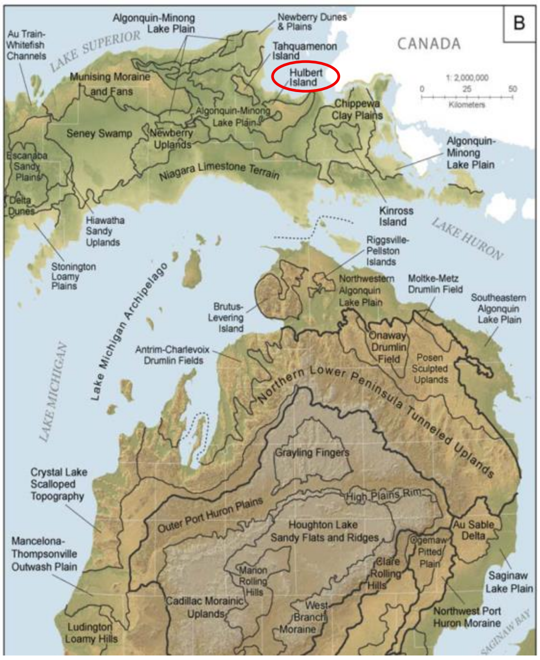

Figure 8: Map showing the Hulbert Island on the Eastern Upper Peninsula Lowlands in Michigan, Source: Schaetzl et al., 2013, Fig. 2.

The study area on Michigan's Upper Peninsula lies in a landscape that was fundamentally shaped by the late Wisconsin glaciation (Larson and Schaetzl, 2001). During the last advance and retreat of the Laurentide Ice Sheet, extensive ground moraines and alluvial plains were deposited in the eastern part of the Upper Peninsula. Deglaciation occurred as the ice margin stagnated and retreated northward, creating a flat relief characterised by moraine plains, meltwater channels and glacial lake deposits (Larson and Schaetzl, 2001). The soils developed primarily in thick, well-sorted glaciofluvial outwash sands, with local influence of glacial deposits derived from mixed sedimentary and crystalline bedrock sources (Derouin et al., 2007). Schaetzl et al. (2020) describe the site as a sandy, well-drained upland in cool, humid climatic conditions under northern forest vegetation. The analysed soils in the study area are primarily Albic Podzols (Šamonil et al., 2016).

In the sandy soils of the Upper Peninsula of Michigan these microtopographies can persist for over 6'000 years (Šamonil et al., 2013). In the studied forest, pit-and-mound features cover 16.9% of the forest with a 12.7% coverage by mounds. Uprooting is the primary disturbance process which affects soil formation in this area (Šamonil et al., 2016). These events affect ecosystem dynamics, the soil formation and erosion and shape the geomorphology of the affected areas (Šamonil et al., 2013). The material that is being accumulated above the pit, tends to erode faster than material in the pit and landscapes with pit and mound structures may have stronger erosion than undisturbed environments (Schaetzl, 1990).

The soils at the study site formed in thick, well-sorted outwash sands that were likely deposited by meltwater near a retreating ice margin. Although the exact age of this glacial position is unsure, it is probably somewhat older than the nearby Munising Moraine to the north, which has been radiocarbon dated to 10'025 ± 100 ^{14}C years BP (Derouin et al., 2007). The area was last glaciated between around 15'500 and 11'500 cal years ago (Schaetzl and Loope, 2008). This suggests that soil formation at the site likely began around 11'500 years ago, or possibly slightly earlier. The site is characterized by a udic soil moisture regime and a frigid soil temperature regime, having cool summers and long, cold, snowy winters (Schaetzl et al., 2020). The site has an annual average of 812 mm of precipitation and a mean annual temperature of 4.7 °C. It is located within a Lake Superior snowbelt, receiving an average of 255 cm of snowfall annually (Schaetzl et al., 2015). Often the average seasonal maximum snow cover is more than 1.25 m. The study site is located in a previously managed forest, which was last cut at least 40 years ago (Šamonil et al., 2016). The secondary forest at this location is dominated mainly by sugar maple (Acer saccharum), with smaller proportions of red maple (Acer rubrum), black cherry (Prunus serotina), white pine (Pinus strobus) and American beech (Fagus grandifolia). According to late 19th-century survey records from the General Land Office, the vegetation of the region prior to settlement consisted mainly of a forest of beech, sugar maple and hemlock (Tsuga canadensis) (Schaetzl et al., 2020). The study area has an elevation of 215-270 m a.s.l. (Šamonil et al., 2013).

2.2 Soil type Albic Podzol

As mentioned, the soils are classified as Albic Podzols according to the WRB (IUSS Working Group WRB, 2022), where typical soil formation processes, called podzolization, take place. This soil-forming process is typical for cool, humid climates, especially under coniferous forests. Podzols are acidic and nutrient-poor soils. Podzols are characterised by a pale leached albic E horizon and a dark spodic B horizon, enriched with organic matter, iron (Fe) and aluminium (Al) (Sauer et al., 2007). The direction of soil development is vertical, due to the sandy soil and the small content of clay (Šamonil et al., 2015). Albic Podzols in the study area are acidic and have a low buffer capacity. Since the Albic Podzol is built on sandy outwash the amounts of iron and aluminium in the soil are low. The pH-value is typically less acidic on the mound than in the pit (Schaetzl et al., 1989). This is mainly because pits accumulate moisture and organic matter, which enhance leaching, the production of organic acids and podzolization. Mounds consist largely of uplifted subsoil material, are better drained and less likely to accumulate fresh litter (Beatty and Stone, 1986; Šamonil et al., 2010). Pits tend to show enhanced acidification, more pronounced eluvial horizons and nutrient loss, while mounds stay less acidic and pedogenetically less advanced (Bronick and Mokma, 2005; Šamonil et al., 2018; Schaetzl et al., 1989). The low buffer capacity allows soil to change faster after a disturbance event and build new horizons faster and organic matter can relocate quicker in the soil (Šamonil et al., 2018, 2010).

These undisturbed Albic Podzols show clear horizons and stable development (Figure 9). A typical Albic Podzol profile consists of an organic-rich surface horizon, a bleached albic E horizon, a spodic B horizon and the characteristic sequence A-E-Bhs-Bs-BC-C (Choma et al., 2021).

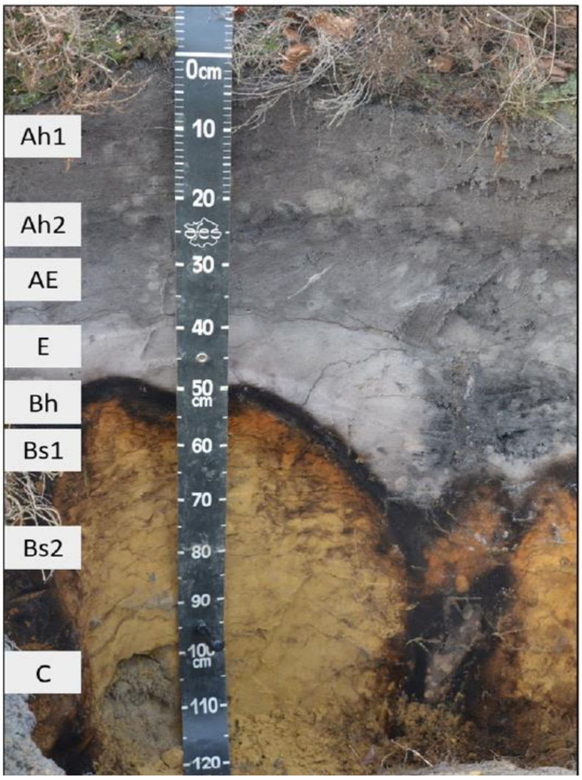

Figure 9: Profile of a typical Albic Podzol with clearly developed soil horizons. Source: Moens et al. (2022), Fig. 1.

In these processes iron, aluminium and organic compounds from the upper A and O horizons are getting washed out. They are shifted downward and deposit in the B horizon. They accumulate in the spodic horizon (Eswaran and Reich, 2005; Sauer et al., 2007) . Fulvates are small, organic molecules which are composed of decomposed plant residues. They can bind easily with metals like Al and Fe, forming organo-metallic complexes (Sauer et al., 2007). The organic components bind with metal elements Al, Fe and humic carbon C in the leaf litter. Then they get transported downwards with water. If they encounter different conditions further down, such as a different pH or other metals, they precipitate, become solid and deposit (Sauer et al., 2007; Tejnecký et al., 2015).

Since most of the examined soils in the study area are disturbed soils, the expected profiles look more like in Figure 10, the horizons are mixed and layers are not well defined. Horizons on disturbed soils need up to >16’000 years to develop the same thickness of a horizon as on an undisturbed site. The development of eluvial and spodic horizon thicknesses indicates that divergent pedogenesis can occur on these small and localised spatial scales (Šamonil et al., 2015).

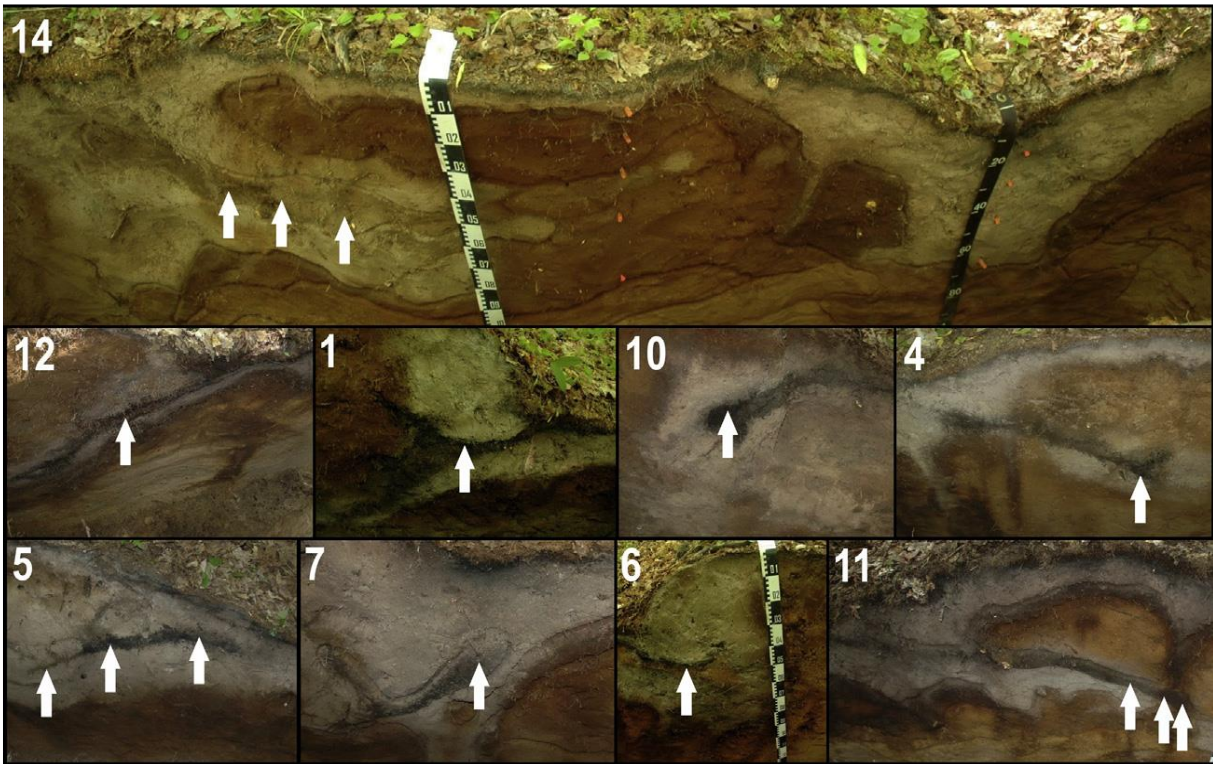

Figure 10: Profiles of a disturbed Albic Podzol, Source: Šamonil et al., 2013, Fig. 5.

3 Materials and Methods

The methods used in this study were selected to answer the research questions. This chapter presents the soil sampling strategy, the sample preparation, the laboratory analyses and the data processing and analysis. The presented methods are based on literature and were used in the past by Šamonil and others working and doing research in this study area. The chapter is divided into several sub-chapters, starting with the soil sampling strategy.

3.1 Soil sampling strategy

Soil sampling was conducted at the end of May and beginning of June 2025 together with the research group of Pavel Šamonil. Overall, 164 soil samples from 5 different sites and depths were collected for this thesis. The 5 study sites are composed of 2 sites at a young mound created by a treethrow, 2 sites at an old mound created by a treethrow and an undisturbed control site over the whole study area. The undisturbed control site should not have been influenced by uprooting or other big disturbance events. The 2 sites at each mound are composed of 1 site directly on the mound and 1 control site, a bit further away, which should not have been affected by uprooting. The young treethrow (treethrow 2) was dated to have been uprooted in the year 1840, giving an age of roughly 180 years for this mound. The old treethrow (treethrow 3) and therefore also the old mound, is dated to have been uprooted about 6’100 years ago (Šamonil et al., 2013). Figure 11 shows an example of a treethrow. At 4 of these 5 study sites, 1 profile and 4 additional mini-profiles for Pu measurements were excavated. At the control site over the whole area only the 4 additional mini-profiles were dug. All soil samples were sampled by depth and not by horizons. This method was chosen, since disturbed soil profiles with turned over and twisted horizons were expected, which would have made it hard to sample by horizon. From the 4 deep profiles samples for meteoric ^{10}Be, in situ ^{10}Be and Portable Optically Stimulated Luminescence (pOSL) were collected. Meteoric ^{10}Be was sampled at 0-10, 10-20, 20-40, 40-60 and 60-90 cm depth. A shovel was used for the sampling and around 500 g of soil was taken for each sample. In total 20 samples of meteoric ^{10}Be were sampled. In situ ^{10}Be was sampled from 0-50 cm, each sample having a weight of around 2’500 g, giving a total of 4 samples for this method. Samples for pOSL were taken in the dark from 0-10, 10-20, 20-40, 40-60 and 60-90 cm with soil cylinders (100 cm^3), giving a total of 20 samples. Each soil cylinder was wrapped with aluminium foil and tape to make sure, no sunlight reaches the sampled soil. From the mini-profiles samples for $^{239+240}$Pu and EA were collected. Pu was collected in depths of 0-5, 5-10, 10-15, 15-20 and 20-25 cm using a soil cylinder (100 cm^3). This is by far the method with the most samples, with a total of 100 soil samples. For EA the same soil samples were used as for $^{239+240}$Pu. For each of the big profiles the horizons were identified and soil properties were described. After collecting the samples, they were opened and dispersed in the house to start drying. At the end of the field trip, all samples were transported to the lab at the University of Zurich for further analysis.

Figure 11: Example of a treethrow feature in the study area. The picture illustrates the pit and mound microtopography, which were sampled.

Profile Treethrow 2 – young Mound and Pit

Treethrow 2 was created around 1840, giving an age of approximately 180 years, which is considered young in this landscape (Šamonil et al., 2013). It is located at 46° 19' 28.66" N and 85° 3' 40.52" W in the forest near Strongs. Treethrow 2 has a north-east facing exposure (33°) and a slope of 9°. As measured in the field, the mound has a height of 70 cm and a slope of 40°.

Profile Treethrow 2 – Control Site young Treethrow

This profile is the control profile for mound 2. The profile was excavated on a flat terrain a few meters away from the mound. The profile doesn't show recent disturbances, which makes it a good control site.

Profile Treethrow 3 – old Mound and Pit

Treethrow 3 was created around 4'077 BCE, giving an age of around 6'100 years (Šamonil et al., 2013). It is located at 46° 19' 25.27" N and 85° 3' 43.00" W in the forest. Treethrow 3 has a north-east facing exposure (35°) and a slope of 7°. This old mound is smaller than mound 2 with a height of around 30 cm and a slope of approximately 10°.

Profile Treethrow 3 – Control Site old Treethrow

This is the control profile for mound 3. Like the profile of mound 2, it was excavated on a flat terrain a few meters away from the mound, where no big disturbances should have occurred recently.

Profile Control Site – Control Site for whole study area

At this site only the 4 mini-profiles were excavated with a soil cylinder (100 cm^3). They were all excavated on flat, undisturbed sites, spaced at regular intervals across an area of 25 m^2. The profiles at this site serve as the control profiles for plutonium over the whole area. The samples were also used for EA.

3.2 Sample preparation

After the samples arrived in the laboratory, they were put in the oven at 40 °C for two days to dry. Both wet and dry mass was noted in a table. The dry samples were sieved with a 2 mm sieve for beryllium and 1 mm sieve for plutonium to separate coarse and fine fragments. 10 grams of the fine material was then milled to samples with a grain size of < 50 µm. This was done with all samples, except the ones for OSL, which needed to be measured immediately and contact with light had to be avoided.

3.3 Laboratory Analyses

This section describes the methods used in this study. The theoretical principles underlying each method are described in chapter 1.3.

3.3.1 Portable Optically Stimulated Luminescence (pOSL)

The portable optically stimulated luminescence was measured to provide luminescence information and identify possible disturbances of the profile. The 20 soil samples were measured in a dark laboratory after removing the aluminium foil in the dark from the soil cylinders. This procedure made sure, that the grains were not exposed to light during transport or the measurements. The measurements were conducted with the SUERC Portable OSL reader (Sanderson and Murphy, 2010). Some material was put in a petri dish, so that the bottom was covered, and then placed in the SUERC Portable OSL reader. The Portable OSL Reader used blue and infrared LEDs for optical stimulation and measured the emitted luminescence signals of quartz and feldspar (Sanderson and Murphy, 2010). The emitted luminescence is measured in total photon counts received after light stimulation in blue (470 nm) and infrared (850 nm), giving values for OSL (quartz) and IRSL (feldspar) (Muñoz-Salinas et al., 2011).

3.3.2 Carbon, Nitrogen and isotope values with Elemental Analysis (EA)

To measure total Carbon (C), total Nitrogen (N) and their isotope ratios, $\delta^{13}C$ and $\delta^{15}N$, elemental analysis was performed using a Thermal Conductivity Detector (TCD). For this the Flash HTC Elemental Analyzer coupled to a Delta V Plus isotope mass spectrometer (IRMS) was used to combust the samples at high temperature and convert them into the gases CO_2 and N_2. Elemental concentrations were quantified using a thermal conductivity detector (TCD), while isotope ratios were measured by the ConFlo IV-Delta V Plus IRMS. The resulting $\delta^{13}C$ and $\delta^{15}N$ isotopic values were calibrated against a Caffeine and Chernozem standard. This was done using 5 mg of material for each of the 100 soil samples and their duplicates.

3.3.3 Long-term erosion rates using Meteoric Beryllium-10

To determine long-term erosion rates concentration of meteoric ^{10}Be was measured in the soil. After all samples were milled, 2 grams of each of the 20 soil samples were analysed in the lab. Organic matter was removed by combusting the samples at 550 °C for 16 hours. Afterwards, Be and other metals were extracted with 16% HCl. ^{9}Be carrier was added to each sample. The samples were shaken, centrifuged and the supernatant was collected. This leaching step was repeated to maximise the Be recovery. After that, the soil samples were further chemically purified by adjusting pH, for example Fe and other concomitant metals were precipitated as hydroxides and the remaining gel was separated by centrifugation. After that, Be and Al were separated by using cation exchange columns. Beryllium was collected. This was then precipitated as hydroxide and converted to BeO at 850 °C. With the Accelerator Mass Spectrometer (AMS) BeO was measured, giving the isotope ratios $^{10}Be/^{9}Be$. Each sample was corrected to the background of the blank. The number of ^{10}Be atoms per sample were calculated using the mass of the known ^{9}Be carrier:

$$N\,^{10}Be = \frac{^{10}Be}{^{9}Be}\;x\;N\,^{9}Be$$

Knowing the mass of the sample, the ^{10}Be concentration was calculated using the following formula:

$$C\,^{10}Be = \frac{N\,^{10}Be}{m_{sample}}$$

where C_{10Be} = concentration of ^{10}Be (atoms/g soil), N_{10Be} = number of ^{10}Be atoms per sample and m_{sample} = mass of the sample (Wittmann et al., 2012).

With the concentration of ^{10}Be, erosion rates for each sample were calculated.

3.3.4 Determining erosion rates using in situ Beryllium-10

To determine erosion rates using surface exposure dating, in situ cosmogenic ^{10}Be concentration was measured in quartz, extracted from the 4 soil samples. After the samples were dried, milled and sieved to grain size fractions of 250-600 µm, organic material and carbonate minerals were removed by treating the samples with aqua regia. Quartz-rich fraction was isolated. This quartz-rich fraction was treated by repeated chemical leaching in diluted HF-HNO_3 solutions to remove meteoric ^{10}Be and remaining feldspar. This process was repeated until the samples reached a stable mass loss, which indicated a sufficient quartz purity (Corbett et al., 2016). Next ^{9}Be was added as a carrier to the samples and quartz was then dissolved in concentrated HF. After quartz was dissolved, beryllium was separated on anion and cation exchange resins. The purified beryllium was precipitated as $Be(OH)_2$ and then ignited to BeO.

After the preparation steps, the ratios of $^{10}Be/^{9}Be$ were measured using an AMS. Blank and standards were measured to monitor background levels and analytical accuracy. The AMS directly measured the following:

$$\left(\frac{^{10}Be}{^{9}Be}\right)_{AMS}$$

The in situ ^{10}Be concentrations were calculated by using the known amount of the added ^{9}Be and the mass of the dissolved quartz. The result is given in atoms per gram of quartz.

$$^{10}\text{Be} = \frac{^{10}Be}{^{9}Be} \times \frac{N^{9}Be}{m_{quartz}}$$

where ^{10}Be = in situ ^{10}Be concentration (atoms/g quartz), N_{9Be} = number of ^{9}Be atoms added as carrier and m_{quartz} = mass of dissolved quartz (g).

3.3.5 Short-term erosion rates using Plutonium

To determine short-term erosion rates, the fallout plutonium isotopes ^{239}Pu and ^{240}Pu were used. A mass of 5 grams of each sample was combusted at 550 °C for 16 hours to remove organic matter. U, Pu and other metals were then extracted from the soil sample with 65% HNO_3. A spike of ^{242}Pu was added to each sample, to apply the isotope dilution technique. The samples were heated at 80 °C to leach Pu from the soil matrix. After shaking, dilution with water and centrifugation the supernatant was filtered and transferred to centrifuge tubes. To separate plutonium, its valency was converted to IV and actinides including plutonium were retained on TEVA resin. After equilibration the resin was collected on a filter and washed. Plutonium was eluted from the resin using 0.05 M ammonium oxalate. The plutonium concentrations were measured using Agilent 8800 inductively coupled plasma mass spectrometer (ICP-MS). Reference soil material (IAEA-447), process blanks and selected duplicates were measured together with the samples. Relying on the known amount of ^{242}Pu in the sample, activity of $^{239+240}Pu$ was calculated, corrected to preparation blanks and normalized to the reference soil material. Erosion rates were then calculated by assuming uniform initial fallout distribution of plutonium.

3.3.6 Soil pH and Bulk Density

The soil pH was measured using a pH electrode from Mettler Toledo. In the lab 10 g of each sample was weighed and mixed with 10 ml of $CaCl_2$. This mixture was then put on a shaker for 30 minutes. After that all samples were centrifuged and the liquid was then ready to be measured with the electrode, giving precise results of pH-values. This procedure was done for 25 representative samples, one profile of each site, by using the same soil which was collected for plutonium.

The bulk density (BD) was calculated using the following formula:

$$BD = \frac{m_{dry\ soil}}{V_{sample}}$$

where m = mass of the sample and V = volume of the sample cylinder (100 cm^3) (Blake and Hartge, 1986).

3.4 Data analyses

All the data was compiled in Excel and analysed in Excel and RStudio. Statistical analyses were performed in RStudio.

For all radionuclides meteoric ^{10}Be, in situ ^{10}Be and $^{239+240}Pu$, inventories were calculated by integrating the measured concentrations or activities over the whole soil profile. For a given layer *i*, the inventory was calculated as follows:

$$I = \sum_i C_i * p_i * \Delta z_i * (1 - S_i)$$

where *I* is the inventory of the respective radionuclide, C_i = measured concentration or activity in layer i, p_i = bulk density of layer I, Δz_i = thickness of the layer and S_i = the volumetric fraction of coarse fragments >2mm.

The meteoric ^{10}Be data was analysed in Excel using two complementary approaches. The method of Lal (2001) was applied, which relates the measured inventory N, atmospheric deposition flux q and radioactive decay constant λ to soil age and inventory loss. The corrected soil age was calculated using the following formula:

$$t_{corr} = -\frac{1}{\lambda} \ln \left(1 - \lambda \frac{N}{q - \rho E m}\right)$$

where N = measured meteoric ^{10}Be inventory, q = atmospheric deposition flux, λ = decay constant, ρ = bulk density, E = erosion rate and m = depth of the topsoil layer. The erosion was then derived from the inventory deficit relative to the expected ^{10}Be accumulation (Lal, 2001). For this approach the first 40 cm of each profile were taken, because mounds are not only expected to have erosion in the topsoil layer.

In the method with Zollinger et al. (2017), the erosion was estimated from the difference between atmospheric input and the effective ^{10}Be inventory. This approach provides a simplified estimate that is normalised to the topsoil layer.

For in situ ^{10}Be, the measured concentrations in quartz were evaluated as indicators of long-term exposure and erosion. The erosion rates were derived knowing an approximate age of the sampled landform. According to Schaetzl et al. (2020) the age of the soil in the study area is around 11’500 years. The erosion rates were calculated with the online CRONUS-Earth exposure age and erosion rate calculator.

For plutonium, the measured $^{239+240}Pu$ activities were first corrected for blanks and chemical recovery using the ^{242}Pu tracer. The corrected inventories of each profile were then compared with the reference inventory from an undisturbed reference site. Plutonium was analysed in Excel by among other using the Solver function. The Lal et al. (2013) approach was directly performed in Excel. For the MODERN approach, the data was transferred to RStudio, where it was further analysed with the MODERN (Modelling Deposition and Erosion Rates with RadioNuclides) model. This model converts fallout radionuclides inventories into quantitative estimates of deposition and erosion. The model compares the depth profile of the reference site with the total inventory of a sampling site. The result of the model is the intersection point along the soil profile. The evolution of the depth is the same for the reference and the sample profile, which is a key assumption of the MODERN model (Arata et al., 2016). As a result, the erosion and deposition rates were calculated and modelled as graphs, including the Integral function S, by MODERN. The erosion/deposition results were given in cm/year over the 62-year period and in t/ha/year. These results were then directly used to compare with the meteoric ^{10}Be and the in situ ^{10}Be erosion results.

The results of the elemental analysis (EA) were plotted in RStudio. Total carbon was evaluated descriptively by depth and site. In addition, a correlation between total carbon and δ^{13}C was plotted as an indicator of potential soil disturbance patterns (Zollinger et al., 2015). Since N was very low and sometimes not detectable, the focus was mainly on C and δ^{13}C.

The pOSL data was processed in Excel, where the OSL and IRSL signal was plotted against the depth of the soil profile. To calculate the IRSL/OSL ratio the following formula was used:

$$IRSL \;/\; OSL\; ratio = \frac{L_{IRSL}}{L_{OSL}}$$

where L_{IRSL} is the luminescence signal measured after infrared stimulation and L_{OSL} is the luminescence signal measured after blue-light stimulation (Sanderson and Murphy, 2010).

The depth trends of the luminescence signals and the ratios were interpreted qualitatively. As portable OSL measurements provide relative luminescence signals, the method was used as an indicator of profile disturbance rather than for absolute age determination.

The soil pH, Alo/Feo and soil bulk density data were analysed descriptively, and pH was plotted by depth and site.

All results were finally compared between the young and old treethrow and between disturbed and undisturbed sites, to assess how mechanical disturbances affect soil properties, soil development and erosion. Clearer horizons, characteristic Podzol horizons, depth patterns of Alo, Feo, pH and carbon were interpreted as further soil development.

4 Results

4.1 Physical and chemical soil characteristics

4.1.1 Soil profiles

Table 2 and Table 3 list the horizons and their depth ranges for the control site, mound and pit of treethrow 2 and 3, respectively. Both treethrows are located on a north-east-facing slope and are in a previously managed forest. The profiles of treethrow 2 (Figure 12, Figure 13 and Figure 14) and treethrow 3 (Figure 15, Figure 16 and Figure 17) differ in their horizon composition and distribution among control site, mound and pit (see Table 2 and Table 3). At treethrow 2, the younger treethrow, the control profile shows a typical Podzol horizon sequence consisting of A, E, Bhs and Bs horizons. The mound shows a simplified horizon structure, which includes an AE and Bw horizon. The pit contains several transitional horizons and deviations from the control site, such as (A)E and B(h)s (Table 2). The profiles of the control site, mound and pit of treethrow 3, the older treethrow, show a clearer and more continuous horizon differentiation. Pit and mound largely follow the typical Podzol horizon sequence, but variations in horizon thickness are present. The control site and the mound show well developed Bhs and Bs horizons and the pit has a massive E horizon (Table 3). All profiles were analysed down to a depth of approximately 1 meter.

Table 2: Profiles of treethrow 2 for control site, mound and pit named with horizon and depth.

Treethrow 2 (Young Treethrow)					
Control Site		**Mound**		**Pit**	
Horizon	**Soil depth (cm)**	**Horizon**	**Soil depth (cm)**	**Horizon**	**Soil depth (cm)**
A	0-1	AE	0-2	A	0-6
E	1-15	Bs	2-12	(A)E	6-15
Bhs	15-32	Bw	12-85	B(h)s	15-23
Bs	32-66	BC	85-100	Bs	23-60
BC	66-92			BC	60-90
(B)C	92+				

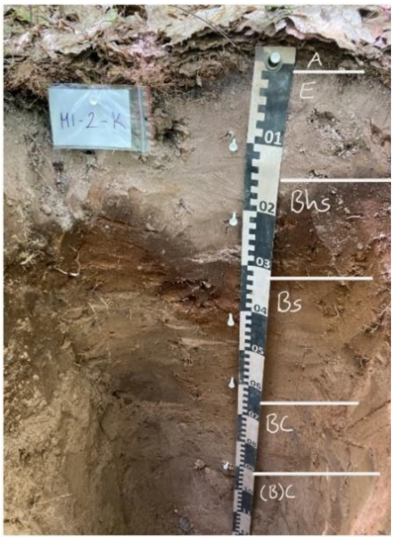

Figure 12: Soil profile of control site 2 with labelled horizons.

Figure 13: Soil profile of mound 2 with labelled horizons.

Figure 14: Soil profile of pit 2 with labelled horizons.

Table 3: Profiles of treethrow 3 for control site, mound and pit named with horizon and depth.

Treethrow 3 (Old Treethrow)					
Control Site		**Mound**		**Pit**	
Horizon	**Soil depth (cm)**	**Horizon**	**Soil depth (cm)**	**Horizon**	**Soil depth (cm)**
A	0-5	A	0-5	A	0-12
E	5-12	E	5-16	E	12-52
Bhs	12-28	Bhs	16-45	Bhs	52-66
Bs1	28-71	Bs	45-93	Bs	66-100
Bs2	71-100	BC	93-115		
BC	100+				

Figure 15: Soil profile of control site 3 with labelled horizons.

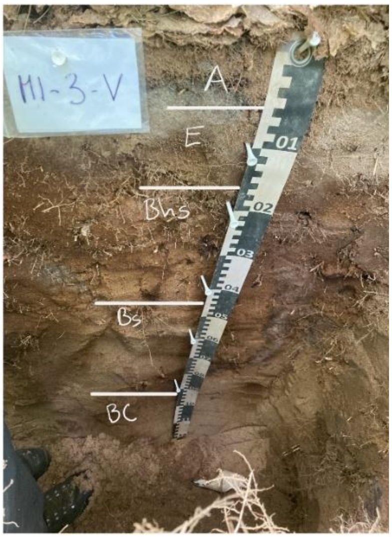

Figure 16: Soil profile of mound 3 with labelled horizons.

Figure 17: Soil profile of pit 3 with labelled horizons.

Overall, the older treethrow 3 exhibits a more clearly differentiated Podzol horizon sequence than the younger treethrow 2, especially in the pit and mound profiles. In contrast, the younger treethrow 2 shows a simplified Podzol profile in the mound and more transitional horizons in the pit.

4.1.2 Skeleton, Bulk Density and pH

The soils in the study area contain a high proportion of sand. All sites show very low to no skeletal content (> 2mm). Only in the pit of treethrow 2 the B(h)s and BC horizons show a very low skeletal content of 1% (see Table 4). For all other horizons and sites, the skeletal content is 0 (Table 4 and Table 5), meaning the soil consists almost entirely of fine earth (< 2mm). The bulk density varies between 0.93 g/cm^3 and 1.50 g/cm^3 between the sites and shows no clear trend with depth, microsite or treethrow age.

The pH values are low across all profiles and horizons, with values between 3.92 and 5.3. The pH increases from acidic surface horizons to less acidic subsoil horizons (see Table 4 and Table 5). The range of the pH between the topsoil (and L and FH horizon) and the subsoil is relatively small.

The soils are consistently sandy, contain almost no skeletal material and show no clear trend in bulk density across sites or horizons.

Table 4: Soils listed by sample depths. Skeleton, bulk density (BD) and pH for profiles of treethrow 2. L and FH in the soil horizon column, stand for L=litter and FH=fermentation+humus. Values for bulk density were rounded to 2 decimal places.

Site	Soil horizon	Soil depth (cm)	Skeleton (%)	BD (g/cm³)	pH
Control Site 2	L	+6.5			4.37
	FH	+5.5			4.45
	A, E	0-10	0	1.19	4.72
	E, Bhs	10-20	0	1.19	4.84
	Bhs, Bs	20-40	0	0.96	5.03
	Bs	40-60	0	1.03	5.18
	Bs, BC	60-90	0	1.31	5.13
	BC, (B)C	90-125	0	1.29	5.02
Pit 2	L	+14.5			4.19
	FH	+12			4.59
	A, (A)E	0-10	0	1.07	4.69
	(A)E, B(h)s	10-20	0	1.15	5.05
	B(h)s	20-40	0	1.22	5.14
	B(h)s	40-60	1	1.28	5.18
	BC	60-90	1	1.44	5.29
Mound 2	L	+1.5			3.92
	FH	+1			4.42
	AE, Bs	0-10	0	1.14	5.18
	Bs, Bw	10-20	0	1.43	5.14
	Bw	20-40	0	1.27	5.19
	Bw	40-60	0	1.28	5.37
	Bw, BC	60-90	0	1.31	5.29

Table 5: Soils listed by sample depths. Skeleton, bulk density (BD) and pH for profiles of treethrow 3. L and FH in the soil horizon column, stand for L = litter and FH = fermentation+humus. Values for bulk density were rounded to 2 decimal places.

Site	Soil horizon	Soil depth (cm)	Skeleton (%)	BD (g/cm^3)	pH
Control Site 3	L	+4			4.44
	FH	+3			4.70
	A, E	0-10	0	1.42	4.71
	E, Bhs	10-20	0	1.25	4.73
	Bhs, Bs_1	20-40	0	1.37	4.97
	Bs_1, Bs_2	40-60	0	1.28	5.10
	Bs_2	60-90	0	1.50	5.12
	Bs_2, BC	90-115	0	1.40	5.11
Pit 3	L	+12			4.64
	FH	+11			4.69
	A	0-10	0	0.93	4.62
	A, E	10-20	0	1.38	4.65
	E	20-40	0	1.26	4.69
	E, Bhs	40-60	0	1.18	5.00
	Bhs, Bs	60-90	0	1.38	5.13
Mound 3	L	+3			3.94
	FH	+2			5.07
	A, E	0-10	0	1.32	4.66
	E, Bhs	10-20	0	1.11	4.88
	Bhs	20-40	0	1.30	5.08
	Bhs, Bs	40-60	0	1.22	5.13
	Bs	60-90	0	1.35	5.14

The pH curve can be seen in Figure 18 (for treethrow 2) and Figure 19 (for treethrow 3). Treethrow 3 has a flatter pH curve than treethrow 2. At treethrow 3 the pH profiles of the three microsites look more similar than at treethrow 2. At both sites the mound generally shows the highest pH along the profile, although the pit of treethrow 2 reaches the same maximum pH of 5.29 at a depth of 60-90 cm. The pH of control site 2 and mound 2 increases until a depth of 40-60 cm and decreases again at a soil depth of 60-90 cm. The pH of the litter (L) and the fermentation + humus (FH) horizons are not shown in the graphs below. The litter horizon (L) is consistently among the most acidic layers. The FH horizon is also acidic, but not always the most acidic horizon in every profile.

To test for significant differences in pH between the two treethrows and between the microsites (control site, mound and pit) a linear mixed-effects model was applied, with depth included as a random factor. The model showed no significant effect of treethrow age on soil pH (p-Value = 0.34, F-Value = 0.46), no significant effect of the microsites (p-Value = 0.64, F-Value = 0.46) and no significant interaction between microsite and treethrow age (p-Value = 0.75, F-Value = 0.29). This indicates that the effect of microsites on soil pH was similar in both treethrows. Variations in pH are largely explained by depth (random-effect variance = 0.1, residual variance = 0.04). Overall, pH values are low across all profiles and the main variation is related to depth rather than to treethrow age or microsite.

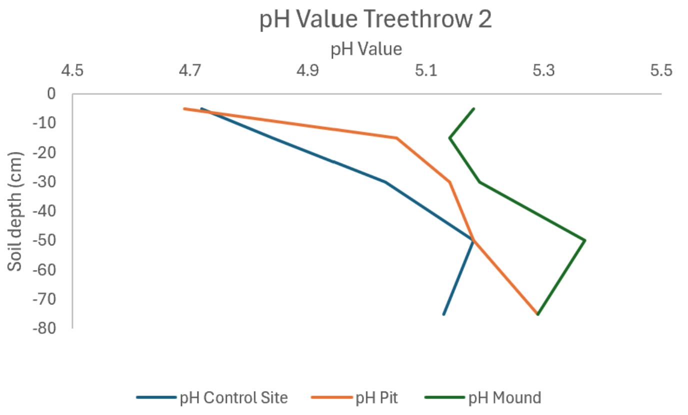

Figure 18: pH curve of mound, pit and control site of treethrow 2.

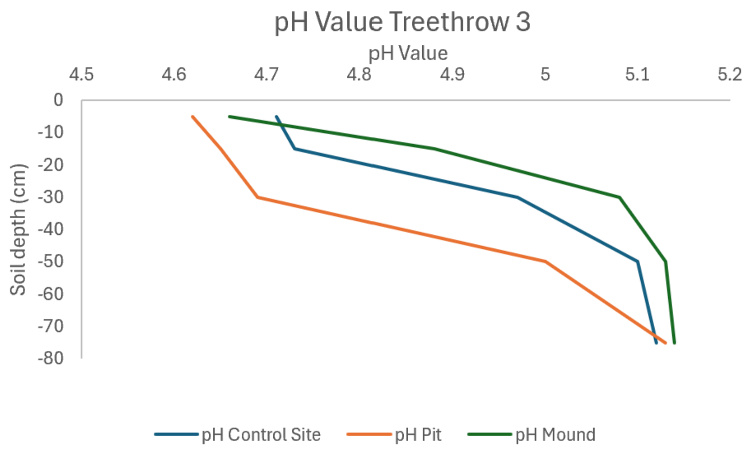

Figure 19: pH curve of mound, pit and control site of treethrow 3.

4.1.3 Feo and Alo

Feo and Alo of all profiles (Table 6 and Table 7) show a clear vertical distribution. The lowest concentrations usually appear in the upper mineral horizons (A, AE, E). The E horizons are strongly depleted in oxalate-extractable Al and Fe, compared to the B horizons. Concentrations are low in the A and E horizons, increase in the spodic B horizons and decrease again in the BC horizons.

The intensity of Feo and Alo accumulation across the soil profile, varies between treethrow 2 (Table 6) and treethrow 3 (Table 7). Treethrow 2 shows overall higher concentrations of Feo and Alo compared to treethrow 3.

At treethrow 2 the control site generally shows the highest concentrations in Feo and Alo. Feo concentrations are lowest in the mound, whereas Alo concentrations are generally lower in the pit than the mound (Table 6). Treethrow 3 shows a similar behaviour where the control site reaches the highest concentration, but there the pit shows much lower concentrations than the mound (Table 7). The control site of treethrow 2 reaches the highest Alo concentration of 5'029.62 mg/kg. The Feo and Alo distributions in all profiles show depletion in the upper mineral horizons and enrichment in the spodic B horizons. The enrichment is higher in the control profiles and at treethrow 2 the concentrations are generally higher than in treethrow 3.

Table 6: Alo and Feo for control site, mound and pit of treethrow 2.

Site	Soil horizon	Soil depth (cm)	Feo (mg/kg)	Alo (mg/kg)
Control Site 2	L	L		
	FH	FH		
	A, E	0-10	160.81	110.48
	E, Bhs	10-20	2338.8	1205.43
	Bhs, Bs	20-40	2930.48	5029.62
	Bs	40-60	1191.66	3449.71
	Bs, BC	60-90	756.19	2159.31
	BC, (B)C	90-125	498.46	824.87
Pit 2	L	L		
	FH	FH		
	A, (A)E	0-10	419.07	159.9
	(A)E, B(h)s	10-20	1126.58	603.97
	B(h)s	20-40	1677.88	1751.15
	B(h)s	40-60	1869.14	3155.81
	BC	60-90	656.05	1165.98
Mound 2	L	L		
	FH	FH		
	AE, Bs	0-10	817.57	2005.46
	Bs, Bw	10-20	859.64	1509.47
	Bw	20-40	736.81	1323.18
	Bw	40-60	1127.19	2381
	Bw, BC	60-90	949.95	2150.55

Table 7: Alo and Feo for control site, mound and pit of treethrow 3.

Site	Soil horizon	Soil depth (cm)	Feo (mg/kg)	Alo (mg/kg)
Control Site 3	L	L		
	FH	FH		
	A, E	0-10	87.97	70.46
	E, Bhs	10-20	2243.99	1994.41
	Bhs, Bs_1	20-40	1854.1	3633.9
	Bs_1, Bs_2	40-60	747.25	1854.25
	Bs_2	60-90	462.85	1127.05
	Bs_2, BC	90-115	353.67	1208.78
Pit 3	L	L		
	FH	FH		
	A	0-10	42.99	34.26
	A, E	10-20	19.31	24.18
	E	20-40	27.18	47.02
	E, Bhs	40-60	308.49	178.34
	Bhs, Bs	60-90	281.27	274.09
Mound 3	L	L		
	FH	FH		
	A, E	0-10	575.64	337.19
	E, Bhs	10-20	1497.1	1724.2
	Bhs	20-40	1068.15	1848.88
	Bhs, Bs	40-60	636.18	1788.11
	Bs	60-90	372.1	1232.58

The Feo and Alo distributions in all profiles show a depletion in the upper mineral horizons and an enrichment in the spodic B horizons. This pattern is most clear in the control profiles, whilst the disturbed pit and mound profiles exhibit a greater variation in enrichment. In general, the concentrations in treethrow 2 are higher than in treethrow 3.

4.1.4 Total carbon, nitrogen and isotopes $\delta^{13}C$ and $\delta^{15}N$

The total carbon (TC) of each site was measured during the elemental analysis (Figure 20). The amount of carbon is low at every site and depth. The measured values range from 0.02% to 3.36% total carbon. In Figure 20 only the mean values of the measured samples are shown. The control sites show a more distinct depth-related pattern, with higher total carbon close to the surface and lower carbon in middle depths, in the eluvial horizon (E horizon) and again higher values in the illuvial B horizon below. Mound 2 shows a more continuous decrease in carbon by depth and mound 3 shows relatively consistent carbon contents for each depth, except between 15 and 20 cm, where a small decrease is visible. However, it increases again in deeper depth. Treethrow 2 (control site and mound 2) show higher contents than treethrow 3 (control site and mound). The control profiles show the clearest depth-related changes in total carbon.

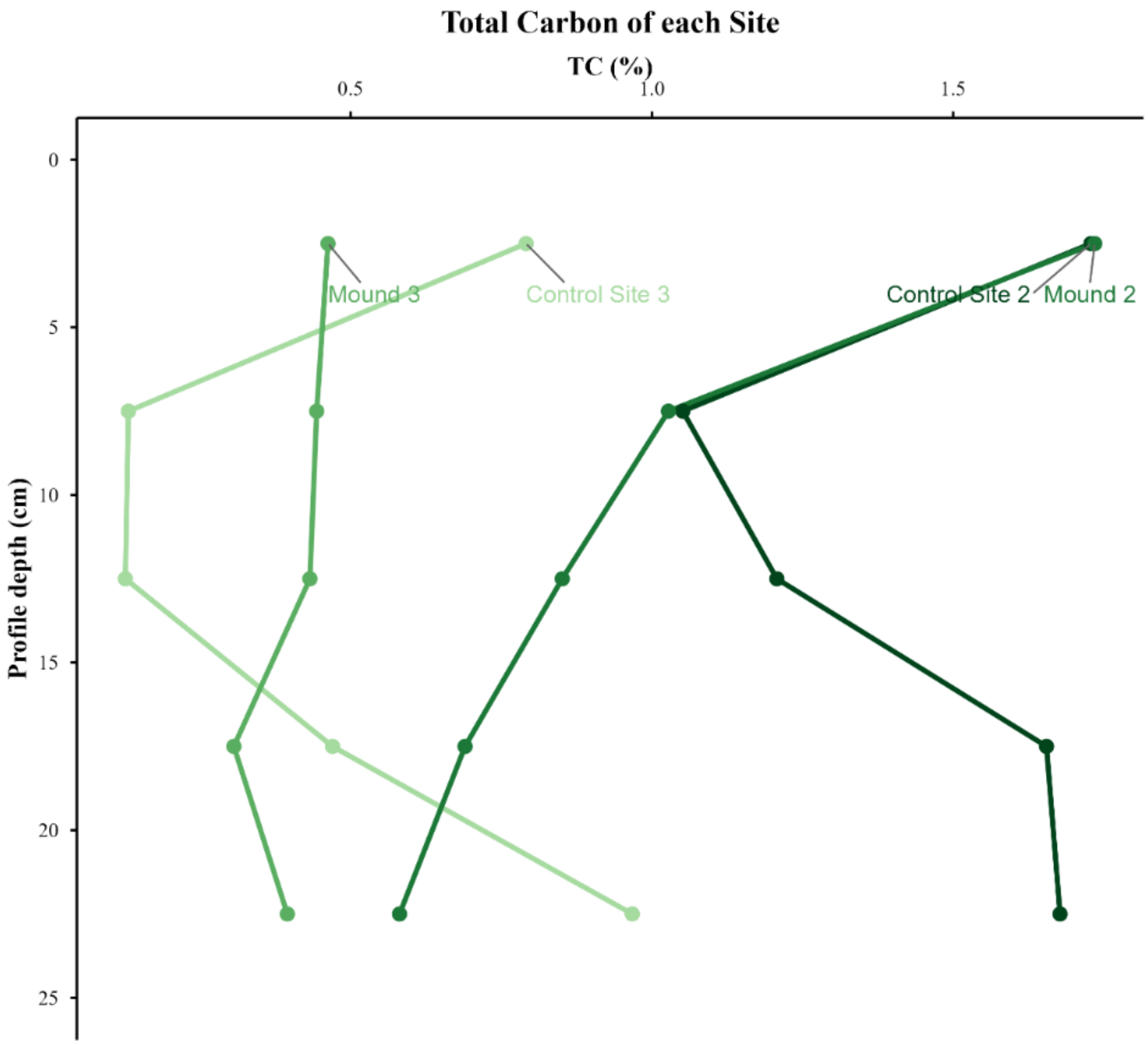

Figure 20: Total Carbon of all sites by depth (0-25 cm). Measured with EA. The mean values per site for each profile were taken.

Below scatterplots for each site are displayed as a qualitative indicator of potential soil disturbance patterns, showing C and $\delta^{13}C$ values (Figure 21, Figure 22, Figure 23, Figure 24, Figure 25). The strength of the linear relationship varies considerably between the profiles. Control site 3 shows the strongest linear fit with a R^2 of 0.934, followed by mound 2 (R^2 = 0.868) and the reference site (R^2 = 0.758). Control site 2 (R^2 = 0.192) and mound 3 (R^2 = 0.274) show much lower linear fits. In contrast to the other profiles, control site 2 shows a positive regression slope and a weak fit, deviating from the general pattern of the other sites, which show negative relationships.

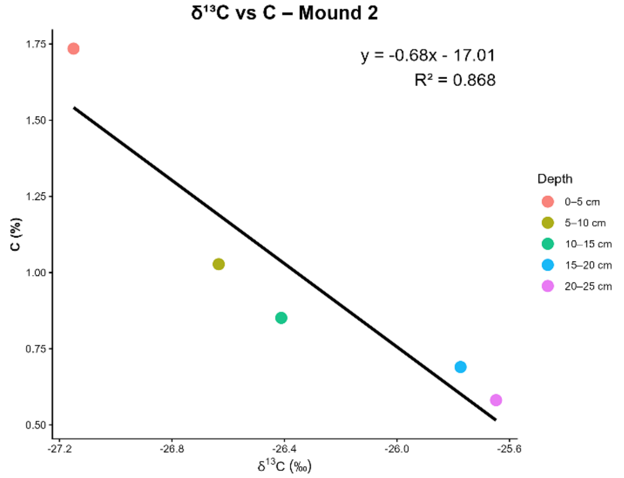

Figure 21: Scatterplot with regression of C (%) and $\delta^{13}C$ of mound 2.

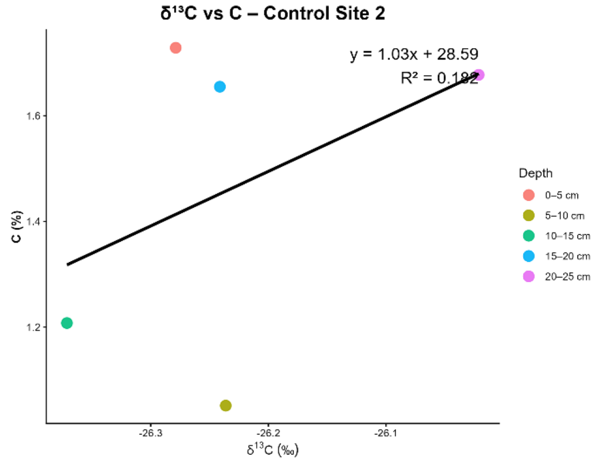

Figure 22: Scatterplot with regression of C (%) and $\delta^{13}C$ of control site 2.

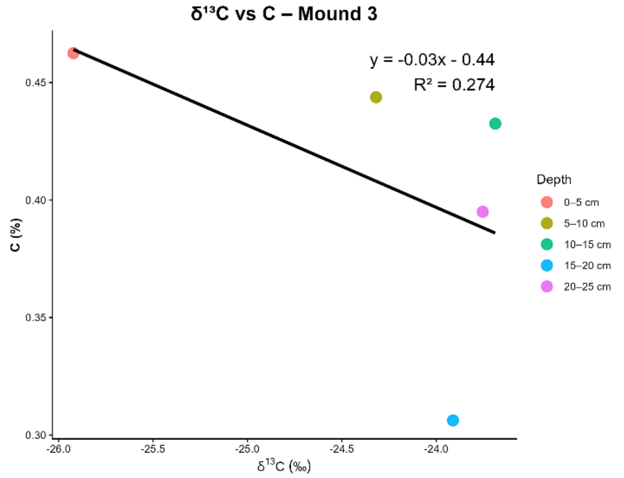

Figure 23: Scatterplot with regression of C (%) and $\delta^{13}C$ of mound 3.

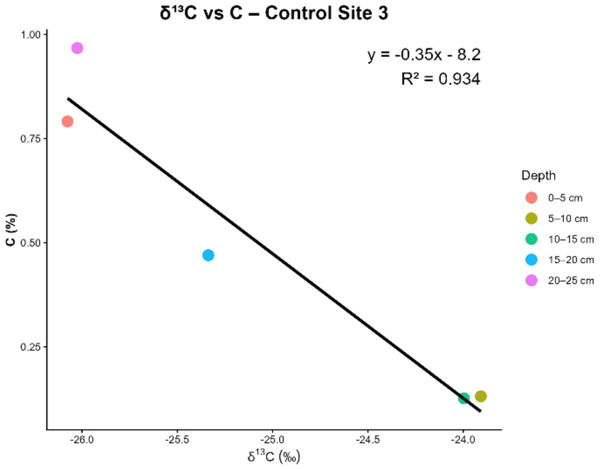

Figure 24: Scatterplot with regression of C (%) and $\delta^{13}C$ of control site 3.

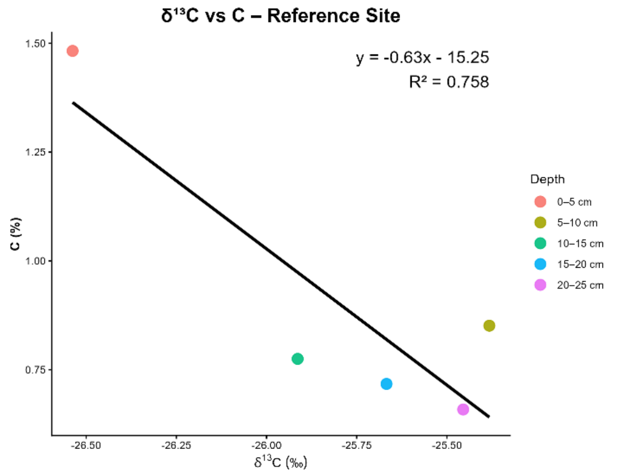

Figure 25: Scatterplot with regression of C (%) and $\delta^{13}C$ of the reference site.

Values for total nitrogen (TN) were generally very low and some were not even detectable by the EA-measurement. The values range from 0.01% - 0.15% total nitrogen in the soil. Overall, there is a tendency that TN values decline with depth, similar to total carbon. The EA results show low C and N contents across all profiles, with the most pronounced depth-specific variations observed in the control profiles, and the C:δ^{13}C ratios varying more significantly between the mound and control sites.

4.2 Portable Optically Stimulated Luminescence (pOSL)

In Figure 26 - Figure 29 the measured OSL (optically stimulated luminescence) and IRSL (infrared stimulated luminescence) intensity-signal for each site is displayed by depth. IRSL represents the signal of feldspar and OSL the signal of quartz minerals. Mound 2 (Figure 26) shows the highest signal intensity at depths between 10 and 60 cm. At depths of 0-10 cm the signal is the lowest and between 60 and 90 cm the signal is also smaller than the signals between 10 and 60 cm. The signal intensity ranges from a luminescence intensity of 984’118 counts (IRSL) at a depth of 0-10 cm to a luminescence intensity of 14’569’163 (net counts of OSL) at a depth of 20-40 cm. The luminescence intensity signal of OSL is higher than the IRSL along the whole profile.

Control site 2 shows a more regular increase in signal intensity with depth, except the signal between 0 and 10 cm (Figure 27), which lies in the middle of the overall signal intensity range. The highest luminescence intensity signal is found at a depth of 60-90 cm and the lowest signal at a depth of 10-20 cm. The luminescence intensity signals vary between 2’330’129 net counts (OSL) at 10-20 cm and 47’817’560 (OSL) at a depth of 60-90 cm. Overall the signals show a higher intensity than the signals captured at mound 2.

At mound 3 low signals were measured between 10 and 60 cm (Figure 28). The highest intensity signal was measured at 60-90 cm, with a photon count of 20’763’462 (IRSL). The lowest count of 461’435 (OSL) was reached by a depth of 20-40 cm. The topsoil layer ranges between these luminescence intensity signals.

The highest signal of control site 3 of 21’115’899 counts (IRSL), is again reached at the deepest layer at a depth of 60-90 cm (Figure 29). The lowest signal of 399’488 counts (OSL) is measured at a depth of 20-40 cm. From a depth of 20-40 cm on to 90 cm, the signal pattern shows a decline with depth. Quartz and feldspar minerals at a depth of 0-20 cm show higher counts than between 20 and 60 cm.

Treethrow 3 shows less clear signal patterns than treethrow 2. Control site 2 shows the strongest and most regular luminescence pattern. Overall, the highest IRSL and OSL intensity signals occur at control site 2. The lowest signals occur at control site 3 and mound 3. Treethrow 3 shows a larger range between the minimum and maximum signal intensities.

The error bars for each measurement were calculated. However, they are so small and negligible that they are not visible in the figures.

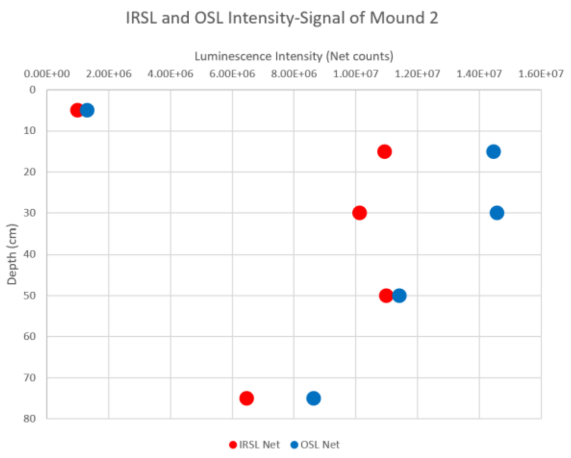

Figure 26: IRSL and OSL Intensity-Signal of mound 2.

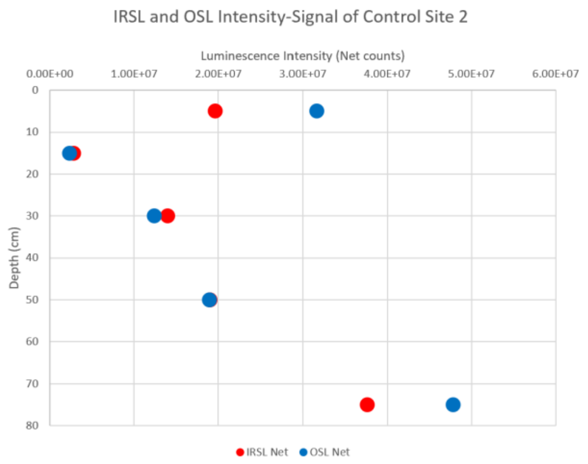

Figure 27: IRSL and OSL Intensity-Signal of control site 2.

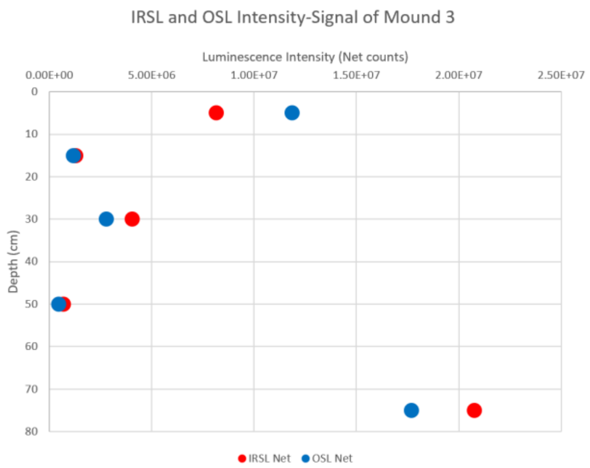

Figure 28: IRSL and OSL Intensity-Signal of mound 3.

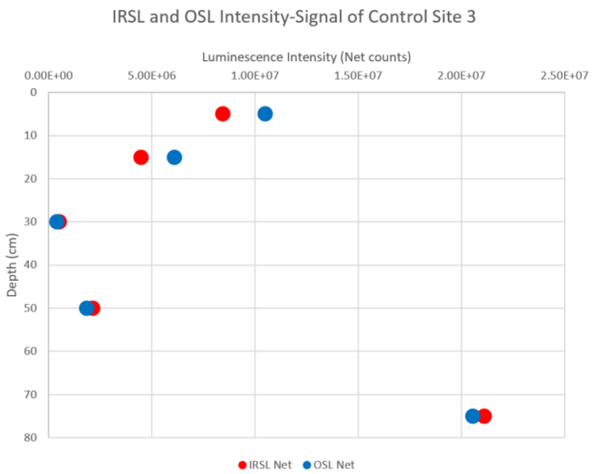

Figure 29: IRSL and OSL Intensity-Signal of control site 3.

To further compare the relative behaviour of quartz and feldspar-related signals, the IRSL/OSL ratio was calculated for each depth. The IRSL/OSL ratio of control site 2 and 3 show a similar pattern (Figure 31 and Figure 33). At both profiles the top layers, at control site 2 from 0-10 cm and at control site 3 from 0-20 cm, show lower ratios, than lower layers. At control site 2 the IRSL/OSL ratio starts to decline from the 10-20 cm layer onwards with a ratio of 1.2 to a ratio of 0.8 in the lowest layer at 60-90 cm. A similar pattern can be seen at control site 3 starting from layer 20-40 cm with a ratio of 1.3 to a ratio of around 1 in the deepest measured layer. Mound 2 shows a similar ratio of around 0.8 along the profile depth (Figure 30). Only between 40-60 cm the ratio is higher, close to 1. Mound 3 shows a different depth ratio pattern, starting at a ratio of around 0.7 at the top layer (Figure 32). The ratio increases to a ratio of 1.4 until a depth of 20-40 cm, where it stays the same for the next deeper layer, until it starts to decrease in the deepest measured layer (60-90 cm) to a ratio of 1.2.

Overall, the luminescence profiles show differences in the regularity of their depth patterns. Control site 2 shows the strongest increase in signal intensity towards deeper layers, while mound 2, mound 3 and control site 3 show more variable signal distributions. The control sites show more similar IRSL/OSL ratio patterns than the mound sites. Mound 3 shows the strongest deviation in the IRSL/OSL ratio profile. These differences indicate that the luminescence depth patterns vary between the sites.

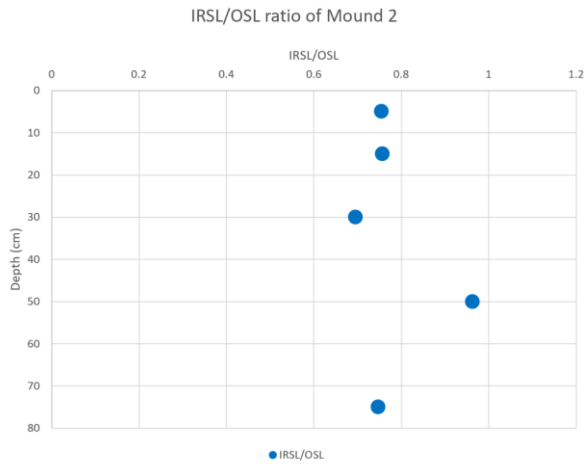

Figure 30: IRSL/OSL ratio of mound 2.

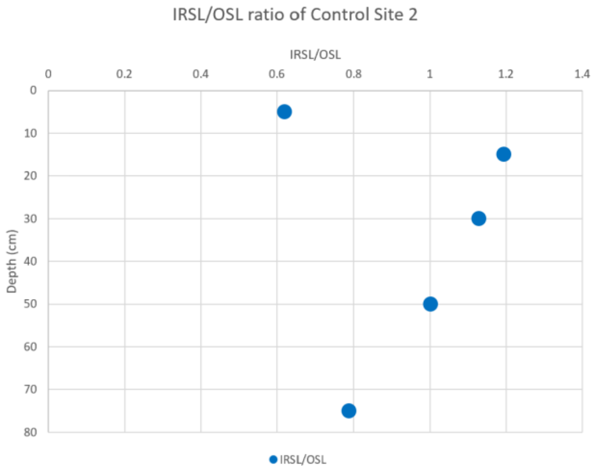

Figure 31: IRSL/OSL ratio of control site 2.

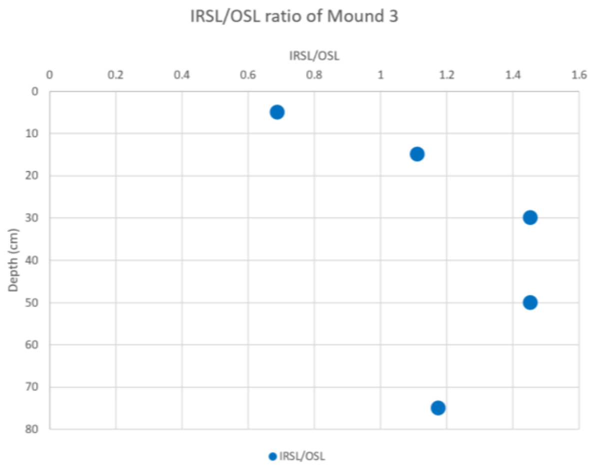

Figure 32: IRSL/OSL ratio of mound 3.

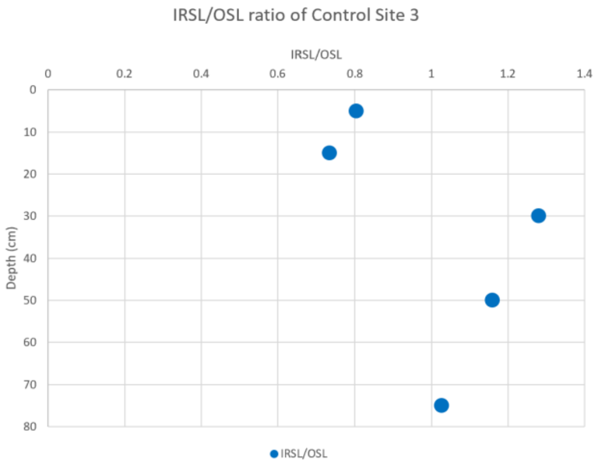

Figure 33: IRSL/OSL ratio of control site 3.

4.3 Meteoric ^{10}Be

4.3.1 Meteoric ^{10}Be concentration and inventory

Below the meteoric ^{10}Be concentration by depth of treethrow 2, with the profiles mound 2 (Figure 30) and control site 2 (Figure 35), and treethrow 3, with the profiles mound 3 (Figure 36) and control site 3 (Figure 33) are shown. Control site 2, mound 3 and control site 3 show a similar pattern across the profile depth, while mound 2 shows a different one.

The by far highest ^{10}Be concentration of mound 2 is reached in the uppermost horizon, between 0 and 10 cm, with a concentration of $3.19*10^8$ ^{10}Be atoms per gram (Figure 34). The concentration drops sharply to $0.5*10^8$ ^{10}Be atoms/g in the underlaying depth layer at 10-20 cm. Further down along the profile the concentration increases again up to $0.79*10^8$ ^{10}Be atoms/g.

In contrast, control site 2 reaches the highest concentration ($2.22*10^8$ ^{10}Be atoms/g) at a depth of 20-40 cm and the lowest concentration ($0.37*10^8$ ^{10}Be atoms/g), near the surface at 0-10 cm. The concentration increases until a depth between 20 and 40 cm and drops in further depths.

Mound 3 shows the lowest concentration between 0-10 cm ($0.13*10^8$ ^{10}Be atoms/g). It increases up to $1.41*10^8$ ^{10}Be atoms/g at a depth of 10-20 cm. After this peak the values drop with increasing depth.

Control site 3 shows a similar pattern, where the smallest ^{10}Be concentration ($0.1*10^8$ ^{10}Be atoms/g) is as well in the layer closest to the surface (0-10 cm). The highest values are found between 10-20 cm ($1.16*10^8$ ^{10}Be atoms/g) and drop after the peak with increasing depth.

The error bars are largest in the uppermost layer of mound 2, mound 3 and control site 3, while control site 2 shows the largest error margin at the middle depth layer.

The profiles at treethrow 2 show higher ^{10}Be concentrations than treethrow 3 across the profile. Mound and control site at treethrow 3 show a more similar pattern than the two profiles at treethrow 2. Mound 2 differs from the other profiles by showing the highest concentration in the uppermost layer.

The total ^{10}Be inventory for each depth layer was calculated by using the horizon thickness, the density and the skeletal content of each horizon. The total profile inventory was gained by summing the inventories of all horizons. Control site 2 and mound 2 show a much higher ^{10}Be inventory than control site 3 and mound 3. The profiles of treethrow 2 show similar inventories, with only a slightly higher inventory at control site 2. In contrast, the profiles at treethrow 3 differ more, where control site 3 shows a higher inventory than mound 3, which has the lowest inventory of all sites (see Figure 36 and Figure 37). At both treethrows, the control site shows higher inventories than the mounds. Treethrow 2 shows generally higher ^{10}Be concentrations and inventories than treethrow 3, while mound 2 differs from the other sites by showing the highest concentration in the uppermost layer. Error bars are small for all sites, indicating low analytical uncertainty of the meteoric ^{10}Be profile inventories.

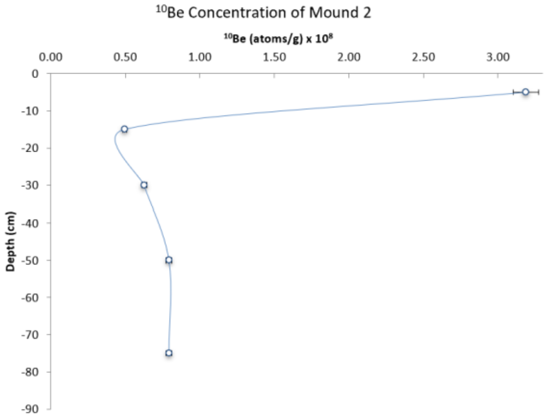

Figure 34: Meteoric ^{10}Be concentration across the profile of mound 2.

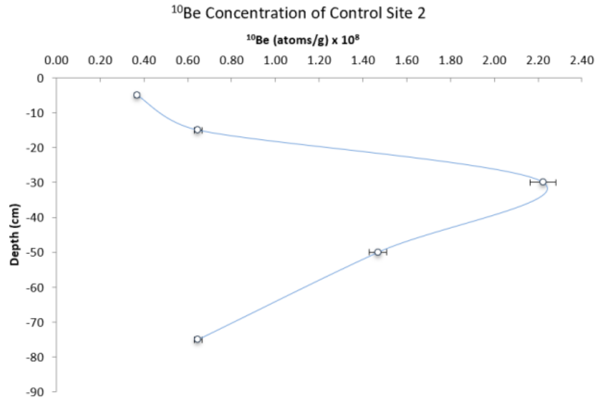

Figure 35: Meteoric ^{10}Be concentration across the profile of control site 2.

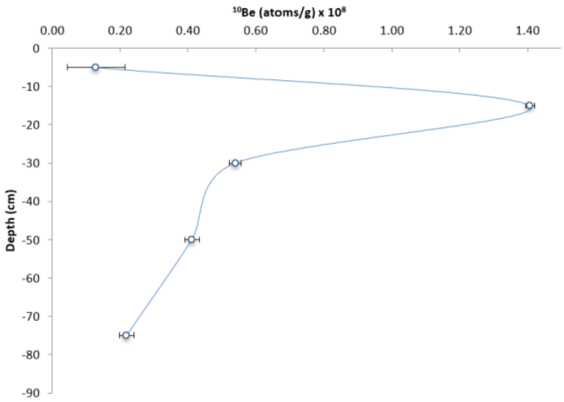

Figure 36: Meteoric ^{10}Be concentration across the profile of mound 3.

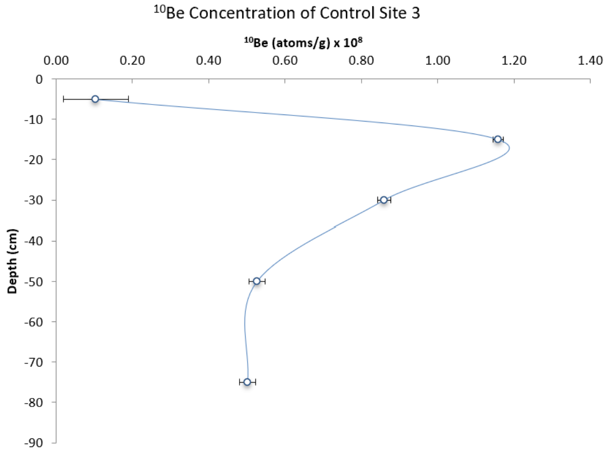

Figure 37: Meteoric ^{10}Be concentration across the profile of control site 3.

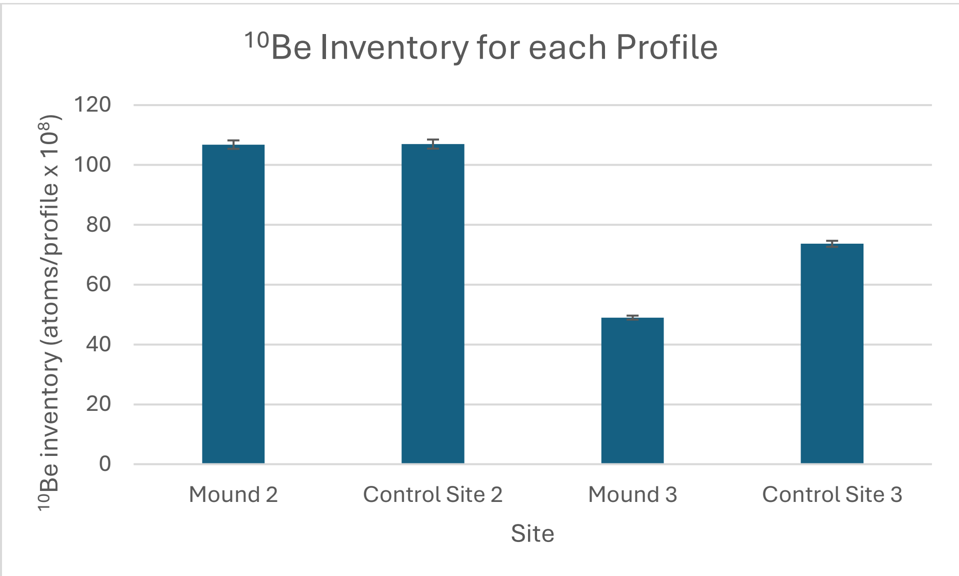

Figure 38: ^{10}Be inventory for each profile at treethrow 2 and 3. The error bars indicate the calculated analytical uncertainty of the meteoric ^{10}Be concentrations for each profile inventory. Uncertainties in bulk density, layer thickness, and skeleton content were not included.

4.3.2 Meteoric ^{10}Be erosion rates

Lower inventories generally correspond to higher calculated erosion rates, while higher inventories correspond to lower erosion rates.

Table 8: Erosion rates calculated from ^{10}Be concentrations with two different methods (Lal (2001) & (Zollinger et al., 2017)). The erosion rates are given in cm/year and t/ha/year for each site. Values are rounded. Negative values show erosion.

Site	Erosion rates using Zollinger et al. (2017)		Erosion rates using Lal (2001)	
	cm/year	t/ha/year	cm/year	t/ha/year
Mound 2	-0.001	-0.101	-0.007	-0.866
Control Site 2	-0.001	-0.108	-0.007	-0.801
Mound 3	-0.033	-4.010	-0.013	-1.566
Control Site 3	-0.009	-1.191	-0.010	-1.343

In Table 8 the calculated erosion rates from concentrations of meteoric ^{10}Be in cm/year and t/ha/year can be seen. Two different methods using Lal (2001) and Zollinger et al. (2017) respectively were used. Figure 39 shows the erosion rates in tons per hectare per year.

Mound 3 shows, using Zollinger et al. (2017), the highest erosion rate by far (Figure 39). Control site 3 has a much lower erosion rate. Mound 2 and control site 2 show very similar and comparatively low values. The Lal (2001) approach shows as well the highest erosion rate of -1.566 t/ha/year for mound 3. Control site 3 has a lower erosion rate compared to mound 3. Mound 2 shows lower erosion than mound 3 and control site 2 shows the smallest erosion of all sites. Lal (2001) shows erosion rates in a more similar range than erosion calculated with Zollinger et al. (2017). Zollinger et al. (2017) shows a much clearer difference between the erosion rates of treethrow 2 and 3, with treethrow 3 having much higher erosion rates Also the pattern between control site and mound with Lal (2001) is similar, with the mound showing slightly higher values. Lal (2001) shows higher erosion rates than Zollinger et al. (2017) for mound 2, control site 2 and control site 3, whereas Zollinger et al. (2017) shows higher values for mound 3 (Figure 39).

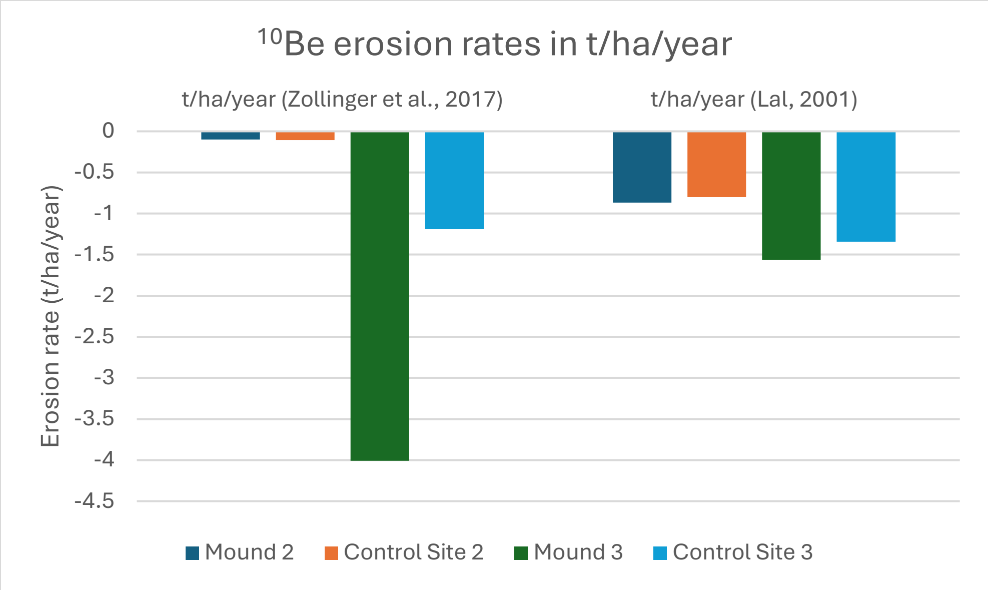

Figure 39: Calculated meteoric ^{10}Be erosion rates in t/ha/year for all sites using both approaches.

Both approaches indicate erosion at all sites, but the rate of erosion differs. In both methods the older treethrow 3 has the sites with the highest erosion rates, whereas treethrow 2 shows lower rates overall. The error of the calculated erosions is estimated to be approximately similar to the errors of the inventory, which showed small errors bars.

4.4 In situ Beryllium

4.4.1 In situ concentration

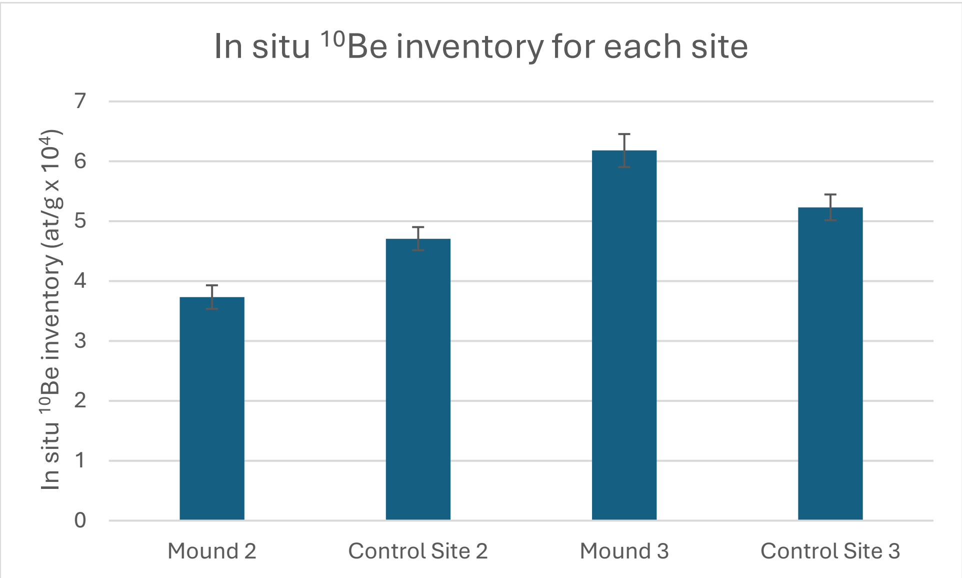

Figure 40: In situ ^{10}Be concentration for each of the 4 sites.

Figure 40 shows that mound 3 has the highest concentration of in situ ^{10}Be, followed by control site 3 and control site 2. Mound 2 has the smallest in situ ^{10}Be concentration. In general, the higher the concentration, the lower the calculated erosion rate.

4.4.2 In situ ^{10}Be erosion rates

Table 9: Erosion rates in cm/year and t/ha/year calculated with in situ ^{10}Be.

Site	Erosion rates	
	cm/year	t/ha/year
Mound 2	-0.0072	-1.1
Control Site 2	-0.00267	-0.4
Mound 3	0	0
Control Site 3	-0.00078	-0.12

In Table 9 the calculated erosion rates of in situ ^{10}Be in cm/year and in t/ha/year are shown.

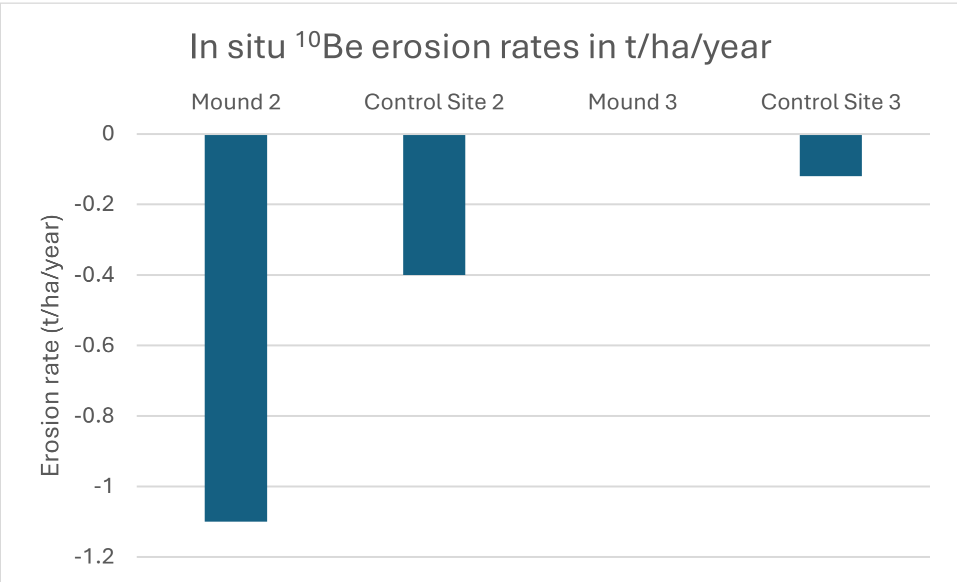

Figure 41: Calculated erosion rates with in situ ^{10}Be for all 4 sites.

The results of the calculated erosion rates for in situ ^{10}Be are shown in Figure 41. The sites that showed a low ^{10}Be concentration in Figure 40 corresponds to higher erosion rates and vice versa. The highest erosion rates are by far calculated for mound 2 (-1.1 t/ha/year), followed by control site 2 (-0.4 t/ha/year) and control site 3 (-0.12 t/ha/year). High concentration of in situ ^{10}Be at mound 3 do not allow to make a plausible conclusion on soil accumulation or erosion, therefore the rate is treated as 0 t/ha/year. The erosion rates are low except for mound 2. The in situ ^{10}Be

results indicate highest erosion at mound 2 and the lowest/no erosion at mound 3, and treethrow 2 shows higher erosion than treethrow 3.

4.5 Plutonium isotopes $^{239+240}Pu$

4.5.1 $^{239+240}Pu$ Inventory

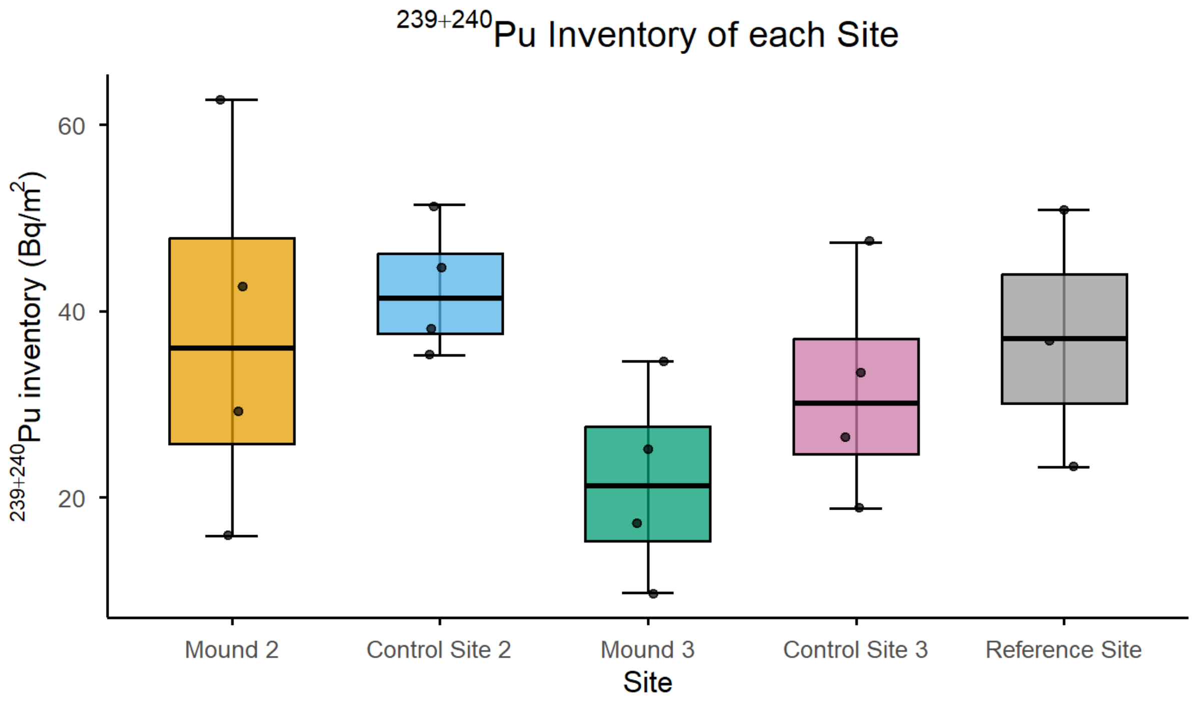

Figure 42: $^{239+240}Pu$ inventory over the whole profile of each site, including the reference site.

In Figure 42 the $^{239+240}Pu$ inventory of each site is shown. The median value is highest at control site 2, followed by the reference site, mound 2, control site 3 and mound 3. Mound 2 shows the biggest variation and control site 2 the smallest. Mound 3, control site 3 and the reference site show a similar, medium high variation.

To calculate the erosion rates based on $^{239+240}Pu$, the MODERN (Modelling Deposition and Erosion Rates with RadioNuclides) model was applied. Plutonium has a reference profile over the whole study area, which is presented in Figure 43.

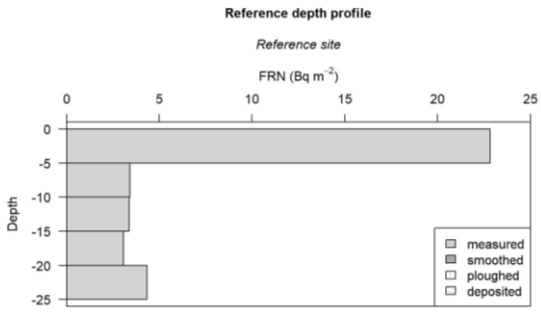

Figure 43: Measured FRN (fallout radionuclides) in Bq/m² by depth of the reference site over the whole study area.

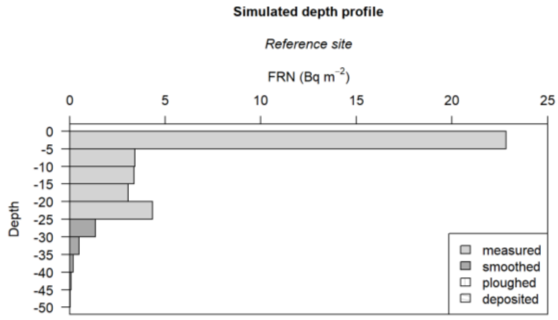

Figure 44: Simulated depth profile of the reference site.

The simulated reference depth profile decreases until the fallout radionuclide activity (FRN (Bq/m²)) approaches 0 (Figure 44). The simulated reference depth profile, created by MODERN, was used as the basis for the following calculations of erosion and accumulation.

4.5.2 $^{239+240}$Pu erosion rates

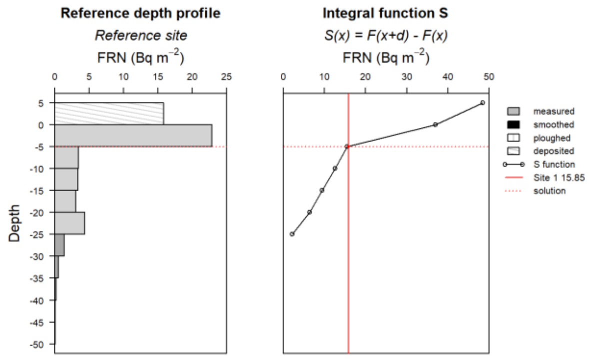

Figure 45: Reference depth profile and Integral function with the erosion rate (red dotted line) of mini-profile 1 of mound 2.

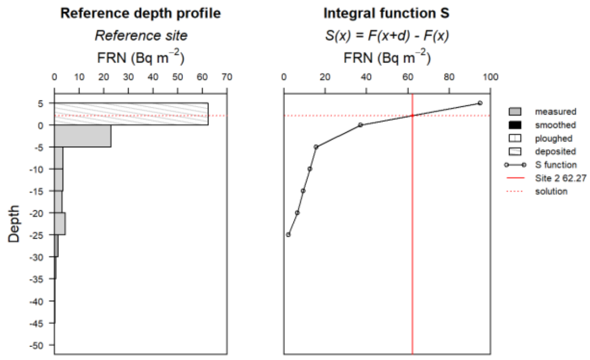

Figure 46: Reference depth profile and Integral function with the accumulation rate (red dotted line) of mini-profile 2 of mound 2.

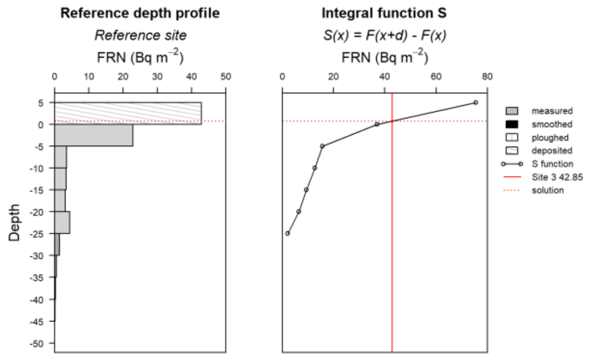

Figure 47: Reference depth profile and Integral function with the accumulation rate (red dotted line) of mini-profile 3 of mound 2.

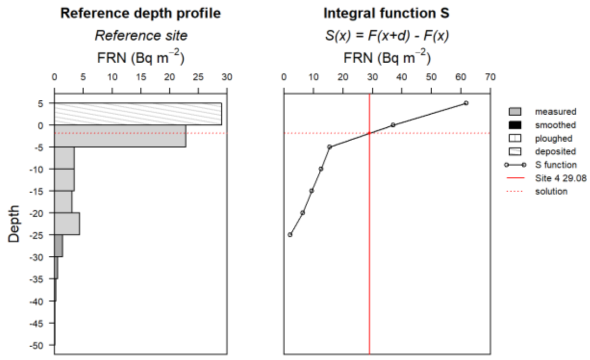

Figure 48: Reference depth profile and Integral function with the erosion rate (red dotted line) of mini-profile 4 of mound 2.

Representative integral function and reference depth profiles of all mini-profiles of mound 2 are shown in Figure 45, Figure 46, Figure 47 and Figure 48. Mini-profile 1 (Figure 45) and 4 (Figure 48) show erosion, while mini-profile 2 (Figure 46) and 3 (Figure 47) show deposition. On average, mound 2 shows erosion.

The plots show the vertical shift of the reference profile required to match the measured inventory of each sample. The model solution is obtained at the x-value where the integral function S equals the total inventory of the sample, and this depth shift is subsequently converted into an erosion or accumulation rate.

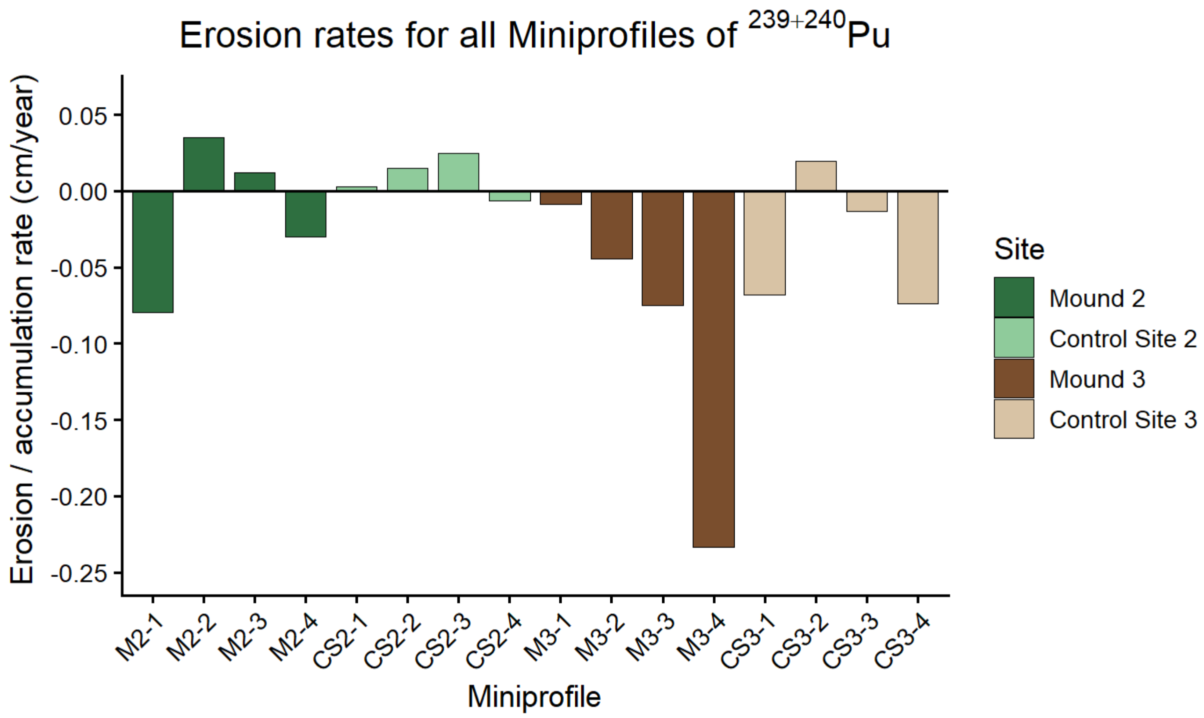

Figure 49: The calculated erosion and accumulation rates in cm/year with MODERN for all mini-profiles (4 per site) are shown.

Figure 49 shows the erosion and accumulation rates of all mini-profiles in cm/year. At mound 2 two profiles show accumulation and two profiles show erosion, with higher values than the accumulation, therefore overall the site shows erosion. Control site 2 shows accumulation at 3 sites and erosion only at one site, resulting on average, in accumulation for this site. All mini-profiles at mound 3 show erosion, although at very different rates. At control site 3 one profile shows accumulation and three profiles show erosion, resulting in erosion overall for this site. On average the mini-profile-based MODERN results show net erosion for mound 2, mound 3 and control site 3, whereas control site 2 shows net accumulation.

Table 10: Erosion rates calculated from $^{239+240}$Pu concentration with MODERN and Lal et al. (2013) for all profiles. Negative values show erosion and positive values show deposition.

Site	Erosion rates using MODERN		Erosion rates using Lal et al. (2013)	
	cm/year	t/ha/year	cm/year	t/ha/year
Mound 2	-0.02	-1.78	-0.02	-3.09
Control Site 2	0.01	1.07	0.03	2.95
Mound 3	-0.09	-14.29	-0.15	-19.95
Control Site 3	-0.03	-3.71	-0.05	-6.18

Table 10 shows the erosion and accumulation rates in cm/year and t/ha/year, measured and modelled with MODERN (Modelling Deposition and Erosion Rates with RadioNuclides) and Lal et al. (2013).

The erosion rates in cm/year calculated from the $^{239+240}$Pu inventory show by far the highest erosion rate for mound 3, followed by control site 3 and mound 2. Control site 3 and mound 2 show a more similar erosion rate than mound 3. Control site 2 even shows slightly accumulation (Figure 50). In Figure 50 the erosion rates are shown in t/ha/year. With MODERN they range from- 14.29 t/ha/year for mound 3, over -3.71 t/ha/year for control site 3 to -1.78 t/ha/year for mound 2. Control site 2 has a slight accumulation of 1.07 t/ha/year (Table 10). Lal et al. (2013) shows the same pattern between the sites but with larger values for all sites, ranging from -19.95 t/ha/year at mound 3 to -3.09 t/ha/year at mound 2, whereas control site 2 again shows with 2.95 t/ha/year accumulation.

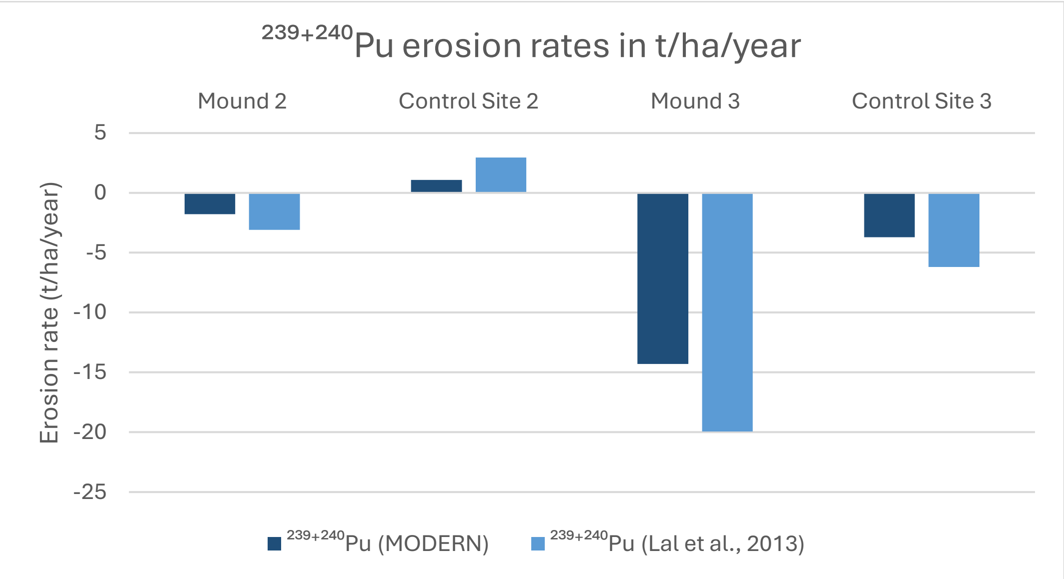

Figure 50: Calculated erosion rates (MODERN and Lal et al., 2013) from $^{239+240}$Pu for all sites in t/ha/year.

The erosion rates calculated with MODERN are lower compared to the ones calculated with the method by Lal et al. (2013) (Table 10 and Figure 50).

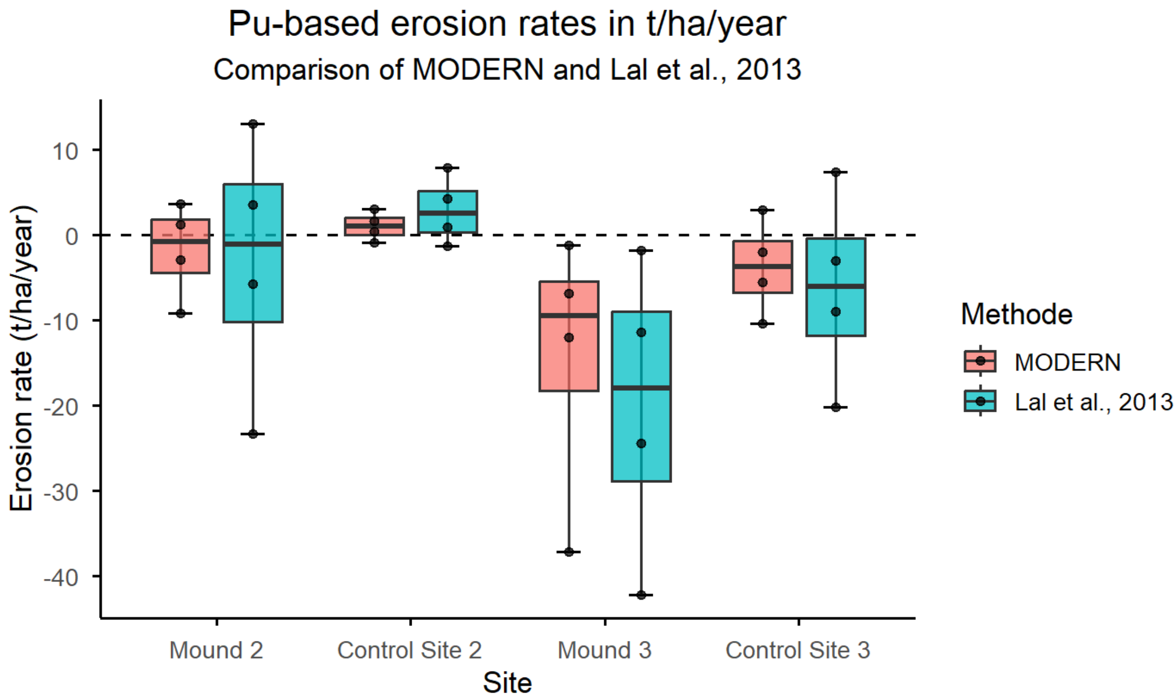

Figure 51: Boxplots of calculated erosion rates with the two Pu-based methods MODERN and Lal et al., 2013.

The boxplots in Figure 51 show greater variability for the results of Lal et al. (2013) than MODERN across all sites. The median of both approaches, MODERN and Lal et al. (2013) lie in the slightly negative range. At control site 2 both medians are in the positive range, and the dispersion is smaller than at the mound sites. Mound 3 shows for both methods the most negative median values. Lal et al. (2013) here shows the highest dispersion and the strongest negative values. At mound 2 and control site 3 the median values are again in the negative range, but not as much as at mound 3.

Paired Wilcoxon signed-rank tests revealed no significant differences at any of the four sites between the Pu-based erosion estimates from MODERN and those from Lal et al. (2013) (all $p > 0.05$). The p-values are 0.855 for mound 2, 0.201 for control site 2, 0.100 for mound 3 and 0.548 for control site 3. The most pronounced difference between the two methods, was observed at mound 3, where Lal et al. (2013) tended to report more negative erosion rates than MODERN, although this difference was not statistically significant.

The Pu-based erosion rates, indicate the strongest erosion by far at mound 3, intermediate erosion at mound 2 and control site 3 and accumulation at control site 2. The results of Lal et al. (2013) produce larger rates and greater variability than the results of MODERN, but they both show the same pattern between the sites.

4.6 Comparison of erosion rates

4.6.1 Comparison of erosion rates of meteoric ^{10}Be and in situ ^{10}Be

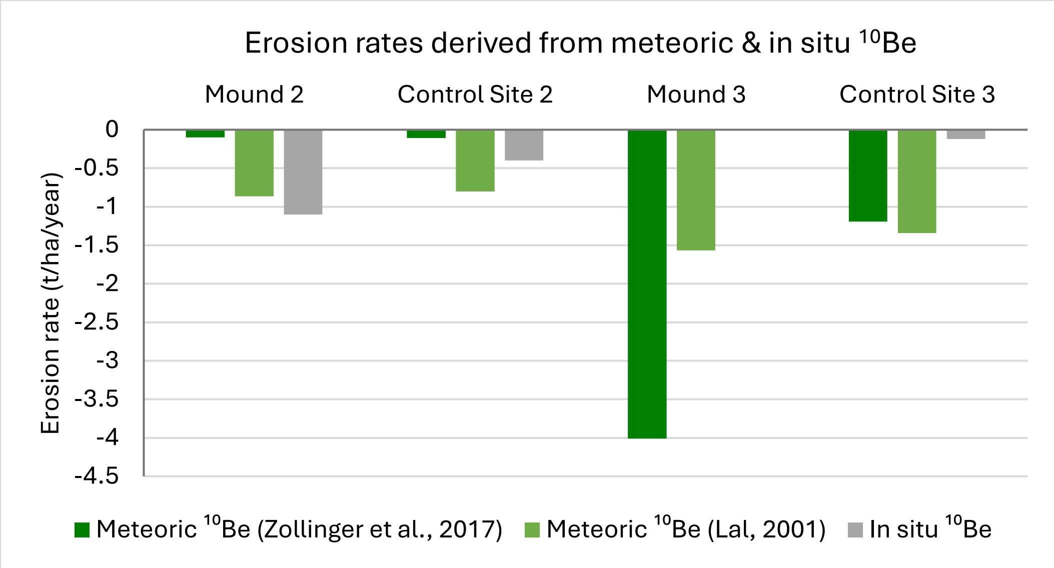

Figure 52: Comparison of erosion rates (t/ha/year) calculated from meteoric ^{10}Be and in situ ^{10}Be.

Figure 52 shows the erosion rates in t/ha/year of meteoric ^{10}Be with the methods (Lal, 2001), Zollinger et al. (2017) and the erosion rates with in situ ^{10}Be. The biggest difference between meteoric and in situ ^{10}Be can be seen at mound 3, where the two approaches of meteoric ^{10}Be show high to very high erosion (compared with the other ^{10}Be results), whereas in situ ^{10}Be shows no measurable erosion. At treethrow 2 all methods show higher erosion at mound 2 than at control site 2. Therefore, meteoric and in situ ^{10}Be show similar patterns at some sites, especially treethrow 2, with in situ ^{10}Be showing the highest rate at mound 2. At treethrow 3 a different pattern is observed, with in situ ^{10}Be showing the smallest erosion values and even no measurable erosion at mound 3.

4.6.2 Comparison of all erosion rates between sites

Figure 53 compares erosion and accumulation rates in t/ha/year derived from meteoric ^{10}Be, in situ ^{10}Be and $^{239+240}$Pu for all four sites. Across all sites, the Pu-based approaches show the highest absolute rates. In situ ^{10}Be yields comparatively low values across all sites and meteoric ^{10}Be small to intermediate values. Both Pu-based approaches show the same pattern, with mound 3 showing by far the strongest erosion, followed by control site 3 and mound 2, whereas control site 2 shows accumulation. The two approaches for meteoric ^{10}Be show more similar erosion rates and are generally lower than the results from $^{239+240}$Pu. They identify mound 3 as the site with the strongest erosion. In situ ^{10}Be shows the strongest deviation from the other methods. At mound 3 it shows no measurable erosion, in comparison to all other methods which show intermediate to high erosion at this site. At treethrow 2 it shows a similar pattern as meteoric ^{10}Be.

The site-specific comparison shows that mound 2 is characterised by low erosion across all methods, control site 2 shows the lowest erosion rates and even net accumulation in the Pu-based approaches, mound 3 shows the strongest erosion with all methods, except in situ ^{10}Be which shows no measurable erosion there. Control site 3 shows low to intermediate erosion with all methods. Although the amount of erosion depends on the specific applied method, the overall pattern across the sites is relatively consistent across most methods. Particularly the old mound 3 is identified by most methods as the one with the most erosion and control site 2 the one with the least erosion and the only one showing accumulation in the Pu-based approaches.

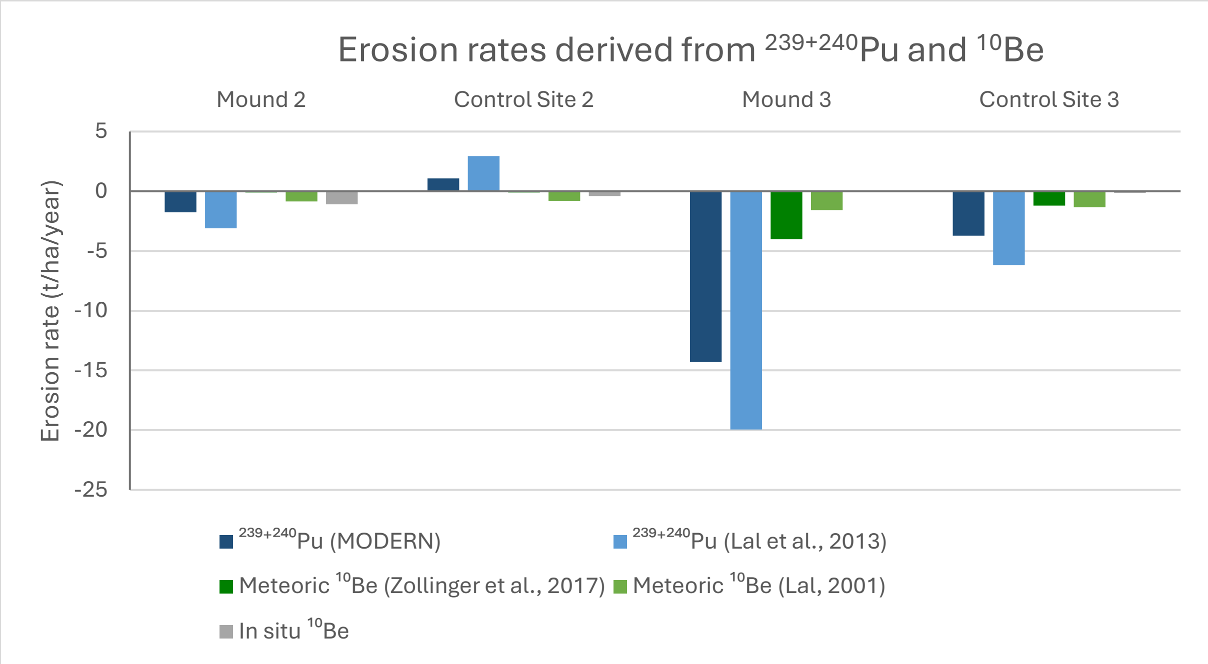

Figure 53: Comparison between erosion rates (t/ha/year) calculated from $^{239+240}Pu$, meteoric 10Be and in situ 10Be. Positive values show deposition and negative values erosion.

Table 11 below gives an overview of all findings across the mounds and control sites. The pits are not listed in the table, since no erosion was measured for them, but they can be found in the results.

Table 11: Summary of the main morphological, geochemical, luminescence and erosion-related findings across the investigated mound and control sites.

Site	Horizon differentiation	pH trend with depth	Feo/Alo pattern	EA pattern (C, N, isotopes)	pOSL signal	$^{239+240}$Pu pattern	Meteoric ^{10}Be pattern	In situ ^{10}Be pattern
Mound 2	Simplified, weak differentiation, disturbed profile	Increasing with depth, less acidic than control site	Weaker spodic differentiation than control, lower concentrations than control site 2	TC decreases with depth, regular negative C: δ^{13}C regression, low C, N	Irregular depth signal, clear disturbance/reworking signal	Intermediate erosion, lower than treethrow 3	Low erosion, slightly higher than control site 2	Highest erosion of all four sites
Control Site 2	Clearer differentiation than mound 2	Increasing with depth	Strongest Feo/Alo enrichment, clearest Podzol pattern	Depth-related TC pattern of Podzols, weak positive C: δ^{13}C regression, low C, N	Most regular and strongest luminescence pattern, increasing with depth	Net accumulation overall	Lowest erosion	Lower erosion than mound 2
Mound 3	Moderate differentiation, clearer, more continuous than mound 2	Increasing with depth, less acidic than control site	More differentiated than mound 2, lower values than treethrow 2	Constant TC with depth, weak negative C: δ^{13}C regression, lower C, N compared to mound 2	Irregular depth signal, weaker pattern compared to mound 2	Strongest erosion of all sites	Strongest erosion of all sites	No measurable erosion, highest in situ 10Be concentration
Control Site 3	Strong, well-differentiated Podzol profile	Increasing with depth	Clearer spodic pattern and higher concentrations than mound 3	Clear depth-related TC pattern, strongest negative C: δ^{13}C fit, lower C, N values than control site 2	Less regular than control site 2,	Intermediate erosion, clearly less than mound 3	Intermediate to high erosion, less than mound 3	Very low erosion

5 Discussion

The study aimed to investigate how mechanical disturbances, especially treethrow events, influence soil properties, soil development and erosion processes in the sandy Albic Podzols of the Upper Peninsula in Michigan. The results are interpreted with respect to the main research question, and focusing on differences between disturbed and undisturbed sites, short- and long-term erosion behaviour and differences between young and old treethrows.

5.1 Evidence of mechanical disturbance in the soil profiles

The soil profiles and portable optically stimulated luminescence data provide qualitative evidence that the investigated soils were mechanically disturbed by treethrows. The disturbance signal is especially clear at the mound of the young treethrow 2, where the profile is greatly simplified, compared to the control site. The control profile shows the typical Podzol sequence A-E-Bhs-Bs-BC-(B)C, whereas the mound has a thin AE horizon over Bs and a thick Bw horizon. This suggests that the original horizon sequence was disturbed and that deeper subsoil material was brought upwards during uprooting. This is consistent with the vertical mixing and horizon sequence described by Schaetzl and Follmer (1990) and Šamonil et al. (2015) for sandy forest soils in the Upper Peninsula affected by treethrow. This interpretation is further supported by the pit of treethrow 2, as it contains transitional horizons such as (A)E and B(h)s and does not show a clearly defined, undisturbed sequence, indicating that the soil profile is not yet fully reorganised and still shows clear traces of soil redistribution (Beatty and Stone, 1986). Mixed and transitional horizons are typical of pit and mound systems after uprooting, as the original soil profile is disturbed and not completely reorganised through subsequent soil formation, as reported by (Šamonil et al., 2015, 2010; Schaetzl, 1986). These soils show mosaics composed of material from different horizons (Bobrovsky and Loyko, 2016). In contrast, the older mound and the older pit of treethrow 3 exhibit more continuous sequences of horizons, A, E, Bhs, Bs and BC, which is much closer to the structure of the undisturbed control site and a typical Albic Podzol. This indicates that soil regeneration and the reorganisation of the profile are more advanced at treethrow 3 (Spasić et al., 2024). However, the old mound still differs from the control site in terms of horizon thickness, showing that the effects of the disturbance have not been completely eliminated (Bobrovsky and Loyko, 2016). This is consistent with previous studies showing that macroturbation caused by treethrow can remain visible for centuries to millennia, although post-disturbance pedogenesis reduces the distinctness of the original disturbance signal (Šamonil et al., 2018, 2015). The luminescence results further support this morphological interpretation. At mound 2, the luminescence signal shows an irregular depth pattern. This irregular pattern differs from control site 2, where the luminescence signal generally increases with depth, which is more typical for a relatively undisturbed profile. Only the uppermost part of the profile deviates slightly from the increasing luminescence-depth trend. This might be because the uppermost horizon in the forest may not be completely bleached because direct light exposure is reduced beneath vegetation and litter cover (Mey et al., 2023; Wallinga, 2002). In relatively undisturbed profiles, a more regular increasing depth trend is expected, while irregular luminescence-depth relationships indicate sediment mixing or reworking. The portable OSL data do not provide absolute ages of disturbances, but they provide qualitative support for profile disturbance and sediment redistribution (Sanderson and Murphy, 2010). A similar contrast is evident in the IRSL/OSL ratios. Both control profiles exhibit comparable depth-dependent patterns, with lower ratios in the upper layers and decreasing ratios in deeper layers, which can be interpreted as a more regular depth behaviour in comparison with the mound profiles (Stang et al., 2012). Mound 2 shows a nearly constant IRSL/OSL ratio across most of the profile, while mound 3 follows a more irregular trend. These deviations from the control profiles imply that the burial and exposure history of the mound sediments has been disturbed by uprooting and following redistribution (Stang et al., 2012). A more similar OSL/IRSL ratio can indicate that quartz and feldspar grains experienced a comparable disturbance, exposure or redistribution. It could also be that the grains were only partially bleached, for example when exposure to sunlight was short or incomplete during the disturbance process (King et al., 2014). Stronger differences between OSL and IRSL signals can reflect more selective bleaching, longer light exposure or more differentiated post-disturbance histories of quartz and feldspar (King et al., 2014; Rhodes, 2011). The luminescence signal from the old mound is less clearly disturbed than the one from the young mound, showing that the original disturbance signal has been partially overprinted by long-term soil development and the reorganisation of the soil profile. This trend is consistent with the weakening of the original treethrow signal, as described by (Šamonil et al., 2015), who showed that the effects of treethrow on soil morphology diminish over time due to post-disturbance pedogenesis. Control site 3 shows a slightly less regular luminescence pattern than control site 2, which could be an indicator that the control profiles may not represent equally undisturbed conditions. The irregular signal might have also been influenced by ice wedges and cryoturbation (Bockheim and Tarnocai, 1998). The profile morphology and luminescence data therefore indicate that mechanical disturbances are a key factor in shaping the internal structure of these soils (Šamonil et al., 2015; Schaetzl and Follmer, 1990).

5.2 Influence of mechanical disturbance on soil properties and soil development

Soil properties and soil development, of soil affected by mechanical disturbance, are mainly influenced through horizon mixing, soil redistribution and profile reorganisation. This observation is also supported by Šamonil et al. (2016) and Šamonil et al. (2018). Changes in soil acidity played only a minor role in this case. All soils were acidic and sandy, and the pH values generally increased with depth. The pH values did not differ significantly between treethrow 2 and 3, nor between the microsites, indicating that pH was controlled more strongly by depth than by mechanical disturbance. This indicates that the overall chemistry of Podzols was not largely disturbed and that podzolisation dominated in the long term (Šamonil et al., 2018). A strong dependence of pH on depth can be expected, since Podzols are acidic soils with vertically differentiated horizons (Lundström et al., 2000; Šamonil et al., 2018; Sauer et al., 2007). As shown in previous studies mounds are often less acidic than pits (Schaetzl et al., 1989). There are several reasons for that. The mound is composed of deeper soil horizons, which were pulled up through the uprooting event. These deeper horizons are usually built of subsoil or in some cases even parent material. Another important reason is the lower organic acid input (Beatty and Stone, 1986). Because of the missing leaf litter, less organic acids are produced, which would further acidify the soil. A third important factor is that mounds are usually better drained, exposed to sunlight and drier than pits (Šamonil et al., 2010). Pits collect organic material and moisture, which makes it a perfect environment for acidic processes (Beatty and Stone, 1986). That podzolisation is still the dominant soil-forming process is further supported by the oxalate-extractable Al and Fe distributions across the profile. Alo and Feo followed the characteristic Podzol pattern with low concentrations in the upper mineral horizon, enrichment in the B horizons and again lower values in the BC horizons (Gómez Armesto et al., 2018). However, the intensity and vertical distribution of Alo and Feo accumulation differed between disturbed and undisturbed sites. The undisturbed sites of both treethrows showed higher Alo and Feo concentrations than the disturbed sites. This is probably due to leaching in the soils. In undisturbed soils, leaching in the upper mineral horizons and illuviation of organic Al and Fe in the spodic horizons proceed over long timespans (Lundström et al., 2000), whereas disturbances disrupt the horizon sequences and result in altered and in this case weakened Feo and Alo patterns (Šamonil et al., 2010). Furthermore, treethrow 2 showed higher Alo and Feo concentrations than treethrow 3. This pattern implies that mechanical disturbance weakened the usual strong enrichment of Alo and Feo in the spodic horizon of disturbed soils (Šamonil et al., 2018). The leaching of Al and Fe in the E horizon and their enrichment in the spodic B horizon reflect the downward translocation of organo-metallic complexes (Sauer et al., 2007). Soluble organic compounds produced during the decomposition of litter promote the transport of Feo and Alo (Schaetzl et al., 2020). However, the higher Alo and Feo concentrations in treethrow 2 were probably not only controlled by age, but also by site-specific factors, such as differences in organic input and hydrological conditions (Šamonil et al., 2010). Pits are generally more differentiated and show further developed pedogenesis. Mounds on the other hand show a delayed and reset stage of soil development (Šamonil et al., 2010). This pattern is consistent with the observed differences in horizonation and Alo/Feo distribution. This observation is supported by previous studies showing that soils of mounds often remain less developed than pits and surrounding undisturbed soils, because they consist of a mixed root-plate and subsoil material and are due to the shape and location, more exposed to drying and erosion (Šamonil et al., 2018; Schaetzl et al., 1990). In contrast, the profiles of the pits indicate a more advanced stage of soil formation than those of the mounds, confirming earlier findings that pits promote the accumulation of organic matter, moisture, leaching, and the formation of new soil horizons following a disturbance (Šamonil et al., 2018, 2010; Schaetzl, 1990). Total carbon contents were generally low across all sites, ranging up to a maximum of 3.36%. Such low amounts of carbon can be expected in Albic Podzols developed on sandy outwash deposits with the strongly leached and sandy character (Dymov et al., 2022). The carbon content of control sites 2 and 3 follow the pattern of Podzol profiles, with high values in the top layer due to the influence of litter and humus, which leads to accumulation of carbon. The eluvial horizon in depths around 10 cm, is reflected by a lower carbon content. The lower carbon content in the E horizon represents the depletion of organic matter due to podzolisation and the downward translocation of dissolved organic compounds and organo-metallic complexes (Sauer et al., 2007; Tejnecký et al., 2015). The accumulation of carbon in the illuvial horizon is also consistent with the character of Podzol development, where organo-metallic material accumulates in the illuvial B horizon. In comparison to the control sites, the mounds do not follow the typical Podzol pattern. The high carbon content near the surface likely reflects litter and humus input, whereas the distribution pattern with depth are indicators for disturbance events, which mixed soil material from different horizons. Overall, the carbon content of the mounds decreased with depth, much more strongly detectable for mound 2. Nevertheless, mound 3 still deviates from the control site and strongly shows the disturbance influence. Treethrow 2 and 3 differ in their carbon contents, with treethrow 2 showing higher values than treethrow 3. This difference might not only reflect disturbance age but also site-specific factors such as litter input or the higher erosion rates of treethrow 3, which could lead to redistribution of carbon. The measured total carbon values of 0.02–3.36% are comparable with the carbon concentrations reported for sandy forest soils and sandy spodosols. Yost and Hartemink (2019) reported average SOC contents in the A horizon of approximately 2.3% (23 g/kg) for sandy forest soils and 2.5% (25 g/kg) for sandy spodosols and said that 90% of sandy A horizons contain less than 3.0% carbon. The lower carbon content of treethrow 3 compared to treethrow 2 therefore probably not only reflects differences in age but could also reflect more erosion and the removal of organic-rich fine material from the older mound. The relationship between total carbon and $\delta^{13}C$ further supports this interpretation. In most profiles, lower carbon contents are associated with less negative $\delta^{13}C$ values, which is consistent with the general trend observed in podzols, where total carbon decreases with increasing depth while $\delta^{13}C$ becomes more enriched, as organic carbon decreases due to decomposition and fractionation processes (Muccio and Jackson, 2009; Zollinger et al., 2015). This relationship is strongest at control site 3, mound 2 and the reference site. The strong correlation at Mound 2 does not necessarily indicate an undisturbed profile, it may rather reflect a newly formed carbon isotope gradient within a disturbed mound. In contrast, the weak correlation at control site 2 could be due to the nonlinear carbon distribution typical of podzols. The weak correlation at Mound 3 could reflect redistribution of organic-rich material or remaining disturbance-induced mixing. The $\delta^{13}C$:C pattern should only be interpreted as a qualitative indicator of disturbance events and not as direct evidence for erosion pattern. The content of nitrogen ranged from 0.01%-0.15%, which was even lower than total carbon. In some samples nitrogen was not even detectable, which aligns with the nutrient-poor and strongly leached character of the soil. The measurements did not contain enough measurable nitrogen to be used as an indicator of soil disturbance in this study.

5.3 Influence of mechanical disturbance on erosion rates

All calculated erosion rates show that mechanical disturbance influenced soil redistribution and soil erosion behaviour at the study sites although the extent of this effect varies depending on the tracer used. The results indicate that mechanical disturbance does not affect all tracers and methods in the same way. Across all sites the Pu-based erosion rates show the strongest signal, with mound 3 reaching by far the highest erosion rate, followed by control site 3 and mound 2, and control site 2 which shows slight accumulation. Since both approaches, MODERN and (Lal et al., 2013) of Pu show high erosion rates, the high values are likely not due to the method approach but rather due to the tracer itself. This pattern is consistent with both approaches, although (Lal et al., 2013) produced higher values and a greater variability. The paired Wilcoxon signed-rank test showed no significant differences between the MODERN and Lal et al. (2013) Pu-based approach at any of the four sites ($p > 0.05$), which implies that the $^{239+240}Pu$ signals are consistent and the high values probably reflect the tracer timescale. In contrast both meteoric ^{10}Be approaches, show lower erosion rates overall and in situ ^{10}Be derived erosion rates are even lower. Over most sites, meteoric ^{10}Be erosion rates show the same pattern as Pu erosion rates. Both meteoric ^{10}Be approaches show the highest values at mound 3 and Lal (2001) shows the lowest values at control site 2, although no accumulation is detected at control site 2. This implies that the meteoric ^{10}Be signal broadly agrees with the Pu results in identifying mound 3 as the site with strongest erosion but integrates erosion over a much longer time, before and after the disturbance, and therefore smoothens disturbance peaks. In situ ^{10}Be shows the strongest deviation from the other methods. It identifies mound 2 as the site with the highest erosion followed by control site 2 and control site 3, while no measurable erosion was calculated for mound 3. However, it should be considered that due to high concentration of in situ ^{10}Be in the sample of mound 3 it didn't allow to make a plausible conclusion on soil accumulation or erosion with the CRONUS-Earth exposure age and erosion rate calculator. That is the reason mound 3 is treated as no erosion nor accumulation. This erosion pattern across the sites is in strong contrast with the $^{239+240}Pu$ and meteoric ^{10}Be methods, which showed the highest erosion at mound 3. The old mound 3 is the site where the methods diverge the most. These differences between the methods indicate that mechanical disturbance can be detected but each method captures a different part of the disturbance history and is based on a different tracer. Plutonium shows erosion since the main fallout in the 1950s and 1960s and in these calculations, of the last 62 years. It is therefore especially sensitive to recent disturbances and short-term surface instability. Plutonium is particularly sensitive to recent disturbances, as it has only been recording erosion since the main phase of radioactive fallout in the 1950s and 1960s, whereas meteoric and in situ ^{10}Be measurements integrate erosion over much longer time periods and can therefore smooth out short-lived disturbance peaks, resulting in a more averaged signal (Siame et al., 2011). Abrupt recent changes in erosion might be more detectable by $^{239+240}Pu$. This difference is particularly important here because the young treethrow 2 partly falls within the Pu timescale, whereas the old treethrow 3 is measured in the Pu record mainly through its later geomorphic traces rather than through the original disturbance event itself. Comparable quantitative erosion values of Podzols in the Upper Peninsula are very rare. Nevertheless, several studies from broadly comparable environments and same soil types make a comparison possible. By comparing the Pu-based erosion rates with erosion rates reported by Šamonil et al. (2020), a partially similar but overall weaker magnitude can be seen. Šamonil et al. (2020), reported soil erosion rates ranging from +1.25 t/ha/year (125 $t/km^2/year$) to -1.96 t/ha/year (-196 $t/km^2/year$), whereas the rates calculated in this thesis reach more negative values, especially at mound 3. Mound 2 has an erosion of -1.778 t/ha/year ($^{239+240}Pu$ approach with

MODERN) which is similar to the lower end of the range of erosion rates in Šamonil et al. (2020). In contrast mound 3 shows much higher erosion rates, between -14.29 t/ha/year (MODERN) and -19.95 t/ha/year (Lal et al., 2013). This shows that the younger mound 2 lies within the range of previously reported erosion rates for treethrow-affected forest soils, whereas the older mound 3 shows much higher erosion. By comparing the in situ ^{10}Be erosion rates with Šamonil et al. (2020) they seem to be in a similar dimension. The values are between -0.58 t/ha/year (-58 t/km^2/year) to -0.76 t/ha/year (-76.3 t/km^2/year) (Šamonil et al., 2020) and 0 to -1.1 t/ha/year for this thesis. The values in the thesis show greater differences for both methods. The comparison should be looked at with caution, since the area of Šamonil et al. (2020) is in a steeper old-growth mountain temperate forest. A similar contrast between short- and long-term tracers was found by Loba et al. (2021) in a loess landscape in Poland. There, long-term erosion rates calculated with in situ ^{10}Be ranged from -0.44 to -0.85 t/ha/year, whereas short-term $^{239+240}$Pu rates ranged from -1.2 to -10.9 t/ha/year and were therefore up to ten times higher. This agrees well with the pattern observed in this thesis, where in situ ^{10}Be produced comparatively low erosion rates (0 to -1.1 t/ha/year), while $^{239+240}$Pu yielded the highest rates (1.071 to -19.95 t/ha/year). Thus, although the Polish study represents an agricultural loess environment and not a forested Podzol system, it supports the interpretation that short-term erosion derived from $^{239+240}$Pu shows stronger recent erosion signals than long-term in situ ^{10}Be approaches (Loba et al., 2021). The study with the most similar pedological features, which also worked in forest Podzols, although on steep backslopes in Southeast Alaska, is from Portes et al. (2024). Their Pu-based soil transport rates are described as negligible, ranging from approximately -0.51 t/ha/year of erosion to +0.43 t/ha/year of deposition. These values are far lower than the stronger Pu signals reported in the thesis, particularly at mound 3 and control site 3. A main reason for the different values is probably that the study site represents local geomorphic disturbances, whereas Portes et al. (2024) worked on deep Spodosols, which are interpreted as indicators of relative slope stability (Portes et al., 2024). Erosion rates of meteoric ^{10}Be of a similar magnitude have been reported for loess soils in southwestern Poland. Kowalska et al. (2023) estimated long-term erosion rates of -0.11 to -3.27 t/ha/year. Although this loess landscape differs from the examined study area here, these values are similar to most of the meteoric ^{10}Be rates calculated in this study. Only the erosion rate of mound 3 (-4.010 t/ha/year) is higher. These comparisons indicate that the observed erosion rates at mound 3 are unusually high for the local environment and are probably due to the ongoing geomorphological activity of the old treethrow microsite. Overall, the erosion rates of treethrow 2 are supported by earlier studies but the erosion rates of treethrow 3 are often higher than in the literature. It should be considered that the studies are not directly comparable, due to the different environment.

H4 is only partly supported. Although the long-term tracers based on ^{10}Be smooth out disturbance peaks, the long-term erosion rates at the disturbed and undisturbed sites do not show the same erosion rates, especially the erosion rates at treethrow 3 disagree with this hypothesis.

5.4 Differences in erosion and soil properties between disturbed and undisturbed sites

This chapter compares how mechanical disturbance influences soil profile structure, soil properties and erosion behaviour at the microsite scale. The clearest difference between disturbed and undisturbed sites is visible in the calculated erosion rates. The Pu-based results show higher erosion rates for the disturbed sites, mound 2 and mound 3 than for the undisturbed control sites 2 and 3. Control site 2, which shows slight accumulation, may have functioned as a small local depression in which fine-grained soil containing Pu and humus from nearby microsites had possibly accumulated (Alewell et al., 2017; Šamonil et al., 2015). The meteoric ^{10}Be results show a broadly similar pattern, although, the erosion rates are very similar for the mound and control site at treethrow 2. In situ ^{10}Be differs from this pattern, with mound 2 showing the highest erosion and no measurable erosion was calculated for mound 3. These results support the interpretation, that disturbed sites are more prone to erosion than undisturbed sites. This pattern is consistent with the observed soil profile patterns, but not all soil properties reflect the disturbance caused by treefall to the same degree. Soil pH was largely similar across the various microsites and showed no significant differences between mound, pit, and control sites or between the two chosen treethrow sites, indicating that pH is primarily depth-dependent and only a weak indicator of disturbance. This is consistent with the generally acidic and vertically differentiated character of podzols, in which pH patterns are strongly determined by horizon depth and podzol formation processes (Lundström et al., 2000; Sauer et al., 2007). Total nitrogen content was also very low at all sites and primarily reflects the nutrient-poor nature of the sandy Podzols. Total carbon showed more pronounced differences in its vertical distribution. The control profiles retained a more typical podzol pattern, while the mound profiles exhibited more altered depth trends, likely due to mixing of horizons and redistribution of organic matter. Feo and Alo provided the clearest differentiation among the chemical parameters. Although all profiles followed the general podzol pattern of depletion in the upper mineral horizons and enrichment in the B horizons, the control sites exhibited the strongest enrichment, while disturbed microsites showed weaker or different enrichment patterns. This shows that the Feo/Alo distribution is better preserved under more stable conditions, whereas mechanical disturbances alter the vertical organization of organo-metallic complexes. Such effects are consistent with previous studies, which showed that tree uprooting mixes formerly organized soil horizons and affects pedogenic development (Šamonil et al., 2015; Schaetzl and Follmer, 1990). Overall, disturbed and undisturbed sites differ more in profile architecture, Feo/Alo organization, carbon depth patterns, and erosion behaviour and less in chemical patterns. These observations shows that the strongest differences between disturbed and undisturbed sites are in erosion behaviour and profile architecture rather than in general chemical properties.

These findings support H3, as disturbed microsites generally show higher erosion rates than undisturbed sites. They also support H1, as disturbed sites show weaker horizon differentiation than undisturbed sites.

5.5 Differences in the effects of disturbance between old and young treethrow sites

The comparison between the young treethrow 2 and the older treethrow 3 show that the effects of mechanical disturbance change over time but do not disappear completely, even 6'100 years after the event. The younger treethrow preserves clearer pedogenetic and morphological evidence of a disturbance event, whereas the older treethrow is characterised more strongly by its long-term geomorphological pattern, especially continued erosion and surface lowering.

The most pronounced age-related differences are evident in the development of the soil profile and in the luminescence behaviour. Treethrow 2 exhibits more pronounced disturbance features, while treethrow 3 shows a more continuous Podzol sequence, suggesting that soil regeneration and profile reorganisation have progressed further over time. The pOSL results support this pattern, with a more pronounced disturbance signal at mound 2 and a less pronounced signal at mound 3, suggesting that the original disturbance was partially overprinted by later soil development. However, the less regular luminescence pattern at control site 3 shows that local variability and the selection of reference sites also need to be considered. The geochemical data show a similar trend. Feo and Alo contrasts between disturbed and undisturbed microsites are more pronounced at treethrow 2, whereas mound and control site are more similar at treethrow 3. This suggests that the more recent treethrow preserves stronger pedogenic contrasts, while the older treethrow was influenced by long-term redistribution, regeneration, and partial homogenization. In contrast, the pH value does not show a clear age-dependent pattern and is therefore less sensitive to disturbance age. The erosion data suggest that soil regeneration and geomorphological degradation do not necessarily occur at the same rate. Both Pu and meteoric ^{10}Be show greater erosion at treethrow 3 than at treethrow 2, even though the profile of the older treethrow has a more developed profile morphology. This suggests that the old mound 3 was subject to long-term surface lowering and erosion, even though its soil profile has partially regenerated. The longevity of pit and mound features in the study area, as well as differences in the original size of the mound and local site conditions, may explain why erosion can persist over long periods (Martin et al., 2013; Šamonil et al., 2016; Schaetzl and Follmer, 1990). The in situ ^{10}Be results do not follow this pattern and should therefore be interpreted with caution, as they may have been affected by sampling uncertainties. The comparison between the two treethrows show that disturbance age of the treethrow not only determines how clearly the original disturbance of the soil profile is still visible, but also how erosion develops over time. Treethrow 2 preserves the clearest pedogenic and morphological traces of recent mechanical disturbance, whereas treethrow 3 shows the stronger long-term erosional signal in $^{239+240}$Pu and meteoric ^{10}Be. This supports H2, as the old treethrow shows a profile that is more similar to the initial Podzol state than the young treethrow, although long-term erosion is still ongoing. At the same time, the results show that old treethrows cannot simply be interpreted as completely recovered soils, because geomorphic degradation can continue even where pedogenic recovery is already advanced. Such a transition is consistent with conceptual models of the development of pits and mounds in podzols of temperate forests, where mounds gradually lose height and undergo renewed pedogenesis, but may continue to be affected by erosion and surface lowering over centuries to millennia (Šamonil et al., 2018; Schaetzl, 1990; Small, 1997). Although disturbance age explains part of the contrast between the treethrows, site-specific conditions and tracer-specific sensitivities need to be considered as well.

5.6 Limitations, implications and future research

This study provides new quantitative insights into the effects of treethrow on soil properties, soil development and erosion in the Upper Peninsula of Michigan. However, several limitations need to be considered when interpreting the results. The first limitation is, that the study is based on only two treethrow pairs, one young and one old one together with their control site. Although it allows to compare different disturbance ages it limits the extent to which the results can be generalized for other treethrows. Also, treethrows can have very different spatial extents and local factors such as mound size, slope, vegetation cover, which all can potentially influence soil properties and erosion rates. The two chosen treethrows are also located close to each other, which makes it harder to make a clear proposition for the whole region or even the whole Upper Peninsula. Another limitation is due to the sampling design and the comparability of the applied tracers. $^{239+240}Pu$, meteoric ^{10}Be and in situ ^{10}Be are combined in the study, these methods give erosion rates over different timescales. As discussed before Pu shows recent fallout-derived redistribution, meteoric ^{10}Be shows long-term erosion and in situ ^{10}Be reflects even longer-term histories of surface exposure and erosion. Although these different timescales are a major strength of the study, they also complicate direct comparison between the methods. Differing results therefore do not necessarily indicate a contradiction but also show that the methods measure different aspects and timescales of the disturbance history of the soil. Especially the in situ ^{10}Be data represents a particular source of uncertainty. Only four samples were analysed, and the samples were collected as bulk material from 0-50 cm. It is therefore not exactly known, how much material originated from which horizon or depth and the sample from mound 3 might have been contaminated during the measurements in the laboratory. These circumstances could be a reason why in situ ^{10}Be does not follow the same pattern as $^{239+240}Pu$ and meteoric ^{10}Be. The data should therefore be interpreted more carefully and should not be used as a main basis, but rather as complementary evidence, when comparing erosion between the treethrows. For the Pu-based erosion rates only 3 of the 4 reference profiles were used for the calculations since the fourth profile showed outlier behaviour with a much higher Pu inventory, which might also be a sign that parts of the reference site were not completely undisturbed since the fallout. Since fallout radionuclide methods depend strongly on the representativeness of the reference inventory, outliers would directly influence the calculated erosion rates. Therefore, removing the outlier profile of the reference site made the erosion rates more reliable and informative. It should also not be neglected, that the sampling was done by fixed depths rather than by soil horizons. As explained this approach was used due to the disturbed turned over soil profiles, which would have made it more difficult to sample by horizon. Nevertheless, sampling by depth might mix materials from different horizons especially at control sites where a clearer horizon stratification exists. As a result, some of the chemical and perhaps also the radionuclides signals may have been smoothed compared with the actual pedological structure of the profiles.

Despite these limitations the study shows some important implications. Overall, the results show that the uprooting of trees should not only be understood as an ecological disturbance but also as a long-term pedological and geomorphological process that generates small-scale heterogeneity in sandy podzol landscapes. The younger treethrow still preserves the clearest evidence of mechanical disturbance of the soil profile, whilst the older treethrow demonstrates that soil regeneration and profile reorganisation can coexist with the ongoing, long-term degradation and erosion of mounds. This means that the effects of uprooting evolve over time and cannot be reduced to a simple short-term disturbance followed by complete recovery. Rather, treethrows contribute to the long-term formation of a mosaic of micro-sites which are at different stages of soil development and have different erosion histories. The present study focuses mainly on the pit-mound scale, but the results suggest that treethrow effects should also be considered at the forest stand scale and, over longer periods, at the landscape scale. The value of combining multiple tracers and soil indicators is highlighted in the study. OSL, profile morphology and chemistry, $^{239+240}$Pu, meteoric and in situ ^{10}Be together provide a much more complete picture of treethrow effects than any single method alone. The combined approach makes it possible to distinguish between recent mechanical disturbance, long-term pedogenic changes and erosion behaviour over different timescales. This is particularly important in landscapes where disturbance signals are sometimes partly overprinted by following soil development. At the same time the results make it clear that future studies should pay particular attention to carrier-specific uncertainties and sampling strategies when interpreting erosion datasets based on multiple methods. The findings also have practical implications for forest management and soil conservation, as they demonstrate that the microtopography created by treethrows contribute to long-term soil heterogeneity and the formation of diverse ecological microsites. Preserving such microtopography can therefore help to maintain natural structural and pedogenic diversity in temperate forest landscapes.

Future research should therefore expand the number of investigated treethrow features and include more young and old sites across the Upper Peninsula. Also, more replicate samples for all ^{10}Be methods should be included. This would show if the patterns observed here are valid over a greater range of mound and pit sizes, forest settings and microtopographic differences. Future work should also include more sampling on pits, because this study primarily focuses on mounds, especially in terms of erosion. Also, the sampling of more Pu reference sites would increase the reliability of calculated short-term erosion rates and minimize the influence of outliers. Overall, more quantitative studies on erosion of pit-mound structures in the Upper Peninsula are still needed, because such datasets are very limited and comparing the calculated erosion rates in this study with other available quantitative data would strengthen the erosion rates validity.

6 Conclusion

This study examined how mechanical disturbance by tree uprooting influences soil properties, soil development, and erosion in sandy Albic Podzols of the Upper Peninsula of Michigan. By comparing a young treethrow, an old treethrow, and nearby undisturbed control sites, both short-term and long-term effects of disturbance could be assessed. The results show that treethrow is not only an ecological disturbance, but also an important pedogenic and geomorphological process that contributes to long-term soil heterogeneity and landscape evolution. The results answer the first research question by showing that treethrow strongly alters soil profile morphology, horizonation, and soil development. The young mound displayed a simplified and mixed profile, indicating strong disturbance and reduced soil development after uprooting. In contrast, the old mound showed clearer horizon differentiation and stronger pedogenic recovery, although it still differed from the undisturbed control site. This demonstrates that the effects of treethrow can persist over very long timescales. In addition, pits and mounds developed differently, while pits tended to show stronger podzolisation and profile differentiation, mounds remained less developed and more affected by physical disturbance and erosion. These findings support H1, which states that disturbed sites show weaker horizon differentiation than undisturbed sites, and they also support H2, because older treethrows tend to align more closely with the typical Podzol-like soil than younger treethrows, even though complete recovery to the undisturbed Podzol state is not reached. The second research question addressed differences in erosion rates and soil development between disturbed and undisturbed sites over short and long timescales. The results show clear differences, although their magnitude depends on the tracer and the considered timescale. Fallout plutonium ($^{239+240}$Pu) showed the highest erosion estimates and therefore most strongly reflected recent soil redistribution, whereas meteoric ^{10}Be and in situ ^{10}Be recorded lower erosion rates reflecting longer-term erosion patterns. At the same time, the results indicate that pedogenic recovery and geomorphological degradation do not necessarily proceed at the same rate, although older treethrows show more developed soil profiles, erosion and mound lowering can continue over longer timescales. The in situ ^{10}Be results should be interpreted more cautiously and serve mainly as complementary evidence. The findings largely support H3, as disturbed sites generally show higher erosion rates than undisturbed sites, especially visible in the erosion rates derived from fallout plutonium. H4 is only partly supported, although soil recovery is evident and long-term erosion rates are lower than the short-term erosion signal, old, disturbed sites still show traces of disturbance, especially in their erosion patterns, rather than fully adapting to undisturbed soils. Highest erosion was observed for the old treethrow. This observation suggests that uprooting has a long-lasting effect on the soil.

A key contribution of this study is the combined use of soil profile observations, pH, Alo/Feo, total carbon, portable OSL and especially $^{239+240}$Pu, meteoric ^{10}Be, and in situ ^{10}Be across treethrow sites of different age. By integrating methods that reflect different timescales, this thesis adds a quantitative perspective to previous research on treethrow in the Upper Peninsula and further supports its importance as a major soil-forming and soil-mixing process in temperate forests. In addition, it relates erosion estimates to observed differences in soil morphology and development, addressing the limited quantitative erosion data for treethrows in the Upper Peninsula. Despite these findings, some limitations remain, including the small number of sampled treethrow features and the different assumptions and timescales associated with the applied tracers. Future research should therefore especially include more pit-and-mound systems and examine erosion in pits. More $^{239+240}Pu$ reference sites would also improve the reliability of short-term erosion estimates. In conclusion, treethrow is a key driver of soil redistribution, pedogenesis, and microtopographic diversity in temperate forest ecosystems. In the sandy Podzols of Michigan's Upper Peninsula, tree uprooting creates a long-lasting mosaic of disturbed and recovering soils which differ in chemical and physical characteristics from undisturbed forest soils.

Literature

Alewell, C., Pitois, A., Meusburger, K., Ketterer, M., Mabit, L., 2017. 239+240 Pu from "contaminant" to soil erosion tracer: Where do we stand? Earth-Science Reviews 172, 107–123. https://doi.org/10.1016/j.earscirev.2017.07.009

Arata, L., Meusburger, K., Frenkel, E., A'Campo-Neuen, A., Iurian, A.-R., Ketterer, M.E., Mabit, L., Alewell, C., 2016. Modelling Deposition and Erosion rates with RadioNuclides (MODERN) – Part 1: A new conversion model to derive soil redistribution rates from inventories of fallout radionuclides. Journal of Environmental Radioactivity 162–163, 45–55. https://doi.org/10.1016/j.jenvrad.2016.05.008

Beatty, S.W., Stone, E.L., 1986. The variety of soil microsites created by tree falls. Can. J. For. Res. 16, 539–548. https://doi.org/10.1139/x86-094

Blake, G.R., Hartge, K.H., 1986. Bulk Density, in: Methods of Soil Analysis. John Wiley & Sons, Ltd, pp. 363–375. https://doi.org/10.2136/sssabookser5.1.2ed.c13

Bobrovsky, M.V., Loyko, S.V., 2016. PATTERNS OF PEDOTURBATION BY TREE UPROOTING IN FOREST SOILS. RJEE 1. https://doi.org/10.21685/2500-0578-2016-1-3

Bockheim, J.G., Tarnocai, C., 1998. Recognition of cryoturbation for classifying permafrost-affected soils. Geoderma 81, 281–293. https://doi.org/10.1016/S0016-7061(97)00115-8

Bronick, C.J., Mokma, D.L., 2005. Podzolization in a Sand Pit in Northern Michigan. Soil Science Society of America Journal 69, 1757–1760. https://doi.org/10.2136/sssaj2004.0119

Choma, M., Šamonil, P., Kaštovská, E., Bárta, J., Tahovská, K., Valtera, M., Šantrůčková, H., 2021. Soil Microbiome Composition along the Natural Norway Spruce Forest Life Cycle. Forests 12, 410. https://doi.org/10.3390/f12040410

Clow, T., Willenbring, J.K., Schaller, M., Blum, J.D., Christl, M., Kubik, P.W., von Blanckenburg, F., 2020. Calibrating a long-term meteoric ^{10}Be delivery rate into eroding western US glacial deposits by comparing meteoric and in situ produced ^{10}Be depth profiles. Geochronology 2, 411–423. https://doi.org/10.5194/gchron-2-411-2020

Corbett, L.B., Bierman, P.R., Rood, D.H., 2016. An approach for optimizing *in situ* cosmogenic 10Be sample preparation. Quaternary Geochronology 33, 24–34. https://doi.org/10.1016/j.quageo.2016.02.001

Derouin, S.A., Lowell, T.V., Hajdas, I., 2007. Landscape Evolution and Deglaciation of the Upper Peninsula, Michigan: An Examination of Chronology and Stratigraphy in Kettle Lake Cores. Journal of Great Lakes Research 33, 875–886. https://doi.org/10.3394/0380-1330(2007)33%5B875:LEADOT%5D2.0.CO;2

Dowell, S.M., Humphrey, O.S., Blake, W.H., Osano, O., Chenery, S., Watts, M.J., 2023. Ultra-Trace Analysis of Fallout Plutonium Isotopes in Soil: Emerging Trends and Future Perspectives. Chemistry Africa 6, 2429–2444. https://doi.org/10.1007/s42250-023-00659-7

Dymov, A.A., Grodnitskaya, I.D., Yakovleva, E.V., Dubrovskiy, Y.A., Kutyavin, I.N., Startsev, V.V., Milanovsky, E.Y., Prokushkin, A.S., 2022. Albic Podzols of Boreal Pine Forests of Russia: Soil

Organic Matter, Physicochemical and Microbiological Properties across Pyrogenic History. Forests 13, 1831. https://doi.org/10.3390/f13111831

Eswaran, H., Reich, P.F., 2005. WORLD SOIL MAP, in: Hillel, D. (Ed.), Encyclopedia of Soils in the Environment. Elsevier, Oxford, pp. 352–365. https://doi.org/10.1016/B0-12-348530-4/00019-9

Fülöp, R.-H., Bishop, P., Fabel, D., Cook, G.T., Everest, J., Schnabel, C., Codilean, A.T., Xu, S., 2015. Quantifying soil loss with in-situ cosmogenic 10Be and 14C depth-profiles. Quaternary Geochronology 27, 78–93. https://doi.org/10.1016/j.quageo.2015.01.003

Gómez Armesto, A., Bibián-Núñez, L., Campillo-Cora, C., Pontevedra-Pombal, X., Arias-Estévez, M., Nóvoa-Muñoz, J.C., 2018. Total mercury distribution among soil aggregate size fractions in a temperate forest podzol. Span. J. Soil Sci. 8, 2637. https://doi.org/10.3232/SJSS.2018.V8.N1.05

Gosse, J.C., Phillips, F.M., 2001. Terrestrial in situ cosmogenic nuclides: theory and application. Quaternary Science Reviews 20, 1475–1560. https://doi.org/10.1016/S0277-3791(00)00171-2

Gruškovnjak, L., 2020. Archaeological remains in soil context. Presented at the Scientific Conference Methodology and Archaeometry, pp. 9–36. https://doi.org/10.17234/METARH.2019.2

Hellmer, M.C., Rios, B.A., Ouimet, W.B., Sibley, T.R., 2015. Ice storms, tree throw, and hillslope sediment transport in northern hardwood forests. Earth Surface Processes and Landforms 40, 901–912. https://doi.org/10.1002/esp.3690

Holz, M., Augustin, J., 2021. Erosion effects on soil carbon and nitrogen dynamics on cultivated slopes: A meta-analysis. Geoderma 397, 115045. https://doi.org/10.1016/j.geoderma.2021.115045

IUSS Working Group WRB. 2022. World Reference Base for Soil Resources. International soil classification system for naming soils and creating legends for soil maps. 4th edition. International Union of Soil Sciences (IUSS), Vienna, Austria.

Jelinski, N.A., Campforts, B., Willenbring, J.K., Schumacher, T.E., Li, S., Lobb, D.A., Papiernik, S.K., Yoo, K., 2019. Meteoric Beryllium-10 as a Tracer of Erosion Due to Postsettlement Land Use in West-Central Minnesota, USA. Journal of Geophysical Research: Earth Surface 124, 874–901. https://doi.org/10.1029/2018JF004720

King, G.E., Robinson, R.A.J., Finch, A.A., 2014. Towards successful OSL sampling strategies in glacial environments: deciphering the influence of depositional processes on bleaching of modern glacial sediments from Jostedalen, Southern Norway. Quaternary Science Reviews 89, 94–107. https://doi.org/10.1016/j.quascirev.2014.02.001

Kowalska, B.J., Egli, M., Vögtli, M., Tikhomirov, D., Łabaz, B., Christl, M., Waroszewski, J., 2023. Meteoric 10Be as a tracer of soil redistribution rates and reconstruction tool of loess–mantled soils (SW, Poland). Geoderma 433, 116451. https://doi.org/10.1016/j.geoderma.2023.116451

Lal, D., 1991. Cosmic ray labeling of erosion surfaces: *in situ* nuclide production rates and erosion models. Earth and Planetary Science Letters 104, 424–439. https://doi.org/10.1016/0012-821X(91)90220-C

Lal, R., 2001. Soil degradation by erosion. Land Degradation & Development 12, 519–539. https://doi.org/10.1002/ldr.472

Lal, R., Tims, S.G., Fifield, L.K., Wasson, R.J., Howe, D., 2013. Applicability of 239Pu as a tracer for soil erosion in the wet-dry tropics of northern Australia. Nuclear Instruments and Methods in Physics Research Section B: Beam Interactions with Materials and Atoms, Proceedings of the Twelfth International Conference on Accelerator Mass Spectrometry, Wellington, New Zealand, 20-25 March 2011 294, 577–583. https://doi.org/10.1016/j.nimb.2012.07.041

Larson, G., Schaetzl, R., 2001. Origin and Evolution of the Great Lakes. Journal of Great Lakes Research 27, 518–546. https://doi.org/10.1016/S0380-1330(01)70665-X

Loba, A., Waroszewski, J., Tikhomirov, D., Calitri, F., Christl, M., Sykuła, M., Egli, M., 2021. Tracing erosion rates in loess landscape of the Trzebnica Hills (Poland) over time using fallout and cosmogenic nuclides. J Soils Sediments 21, 2952–2968. https://doi.org/10.1007/s11368-021-02996-x

Lundström, U.S., van Breemen, N., Bain, D., 2000. The podzolization process. A review. Geoderma 94, 91–107. https://doi.org/10.1016/S0016-7061(99)00036-1

Lutz, H.J., Griswold, F.S., 1939. The influence of tree roots on soil morphology. American Journal of Science 237. https://doi.org/10.2475/ajs.237.6.389

Martin, Y.E., Johnson, E.A., Chaikina, O., 2013. Interplay between field observations and numerical modeling to understand temporal pulsing of tree root throw processes, Canadian Rockies, Canada. Geomorphology 200, 89–105. https://doi.org/10.1016/j.geomorph.2013.04.017

Meusburger, K., Mabit, L., Ketterer, M., Park, J.-H., Sandor, T., Porto, P., Alewell, C., 2016. A multi-radionuclide approach to evaluate the suitability of 239+240Pu as soil erosion tracer. Science of the Total Environment, 566-567, 1489-1499. https://doi.org/10.1016/j.scitotenv.2016.06.035

Mey, J., Schwanghart, W., de Boer, A.-M., Reimann, T., 2023. Differential bleaching of quartz and feldspar luminescence signals under high-turbidity conditions. Geochronology 5, 377–389. https://doi.org/10.5194/gchron-5-377-2023

Moens, C., Dondeyne, S., Panagea, I., Smolders, E., 2022. Depth profile of colloidal iron in the pore water of an Albic Podzol. European Journal of Soil Science 73, e13305. https://doi.org/10.1111/ejss.13305

Muccio, Z., Jackson, G.P., 2009. Isotope ratio mass spectrometry. Analyst 134, 213–222. https://doi.org/10.1039/B808232D

Muñoz-Salinas, E., Bishop, P., Sanderson, D.C., Zamorano, J.-J., 2011. Interpreting luminescence data from a portable OSL reader: three case studies in fluvial settings. Earth Surface Processes and Landforms 36, 651–660. https://doi.org/10.1002/esp.2084

Nelson, Lee-Ann, Sanborn, Paul, Cade-Menun, Barbara, J., Walker, J., Olav, Lian, B., 2021. Pedological trends and implications for forest productivity in a Holocene soil chronosequence, Calvert Island, British Columbia, Canada [WWW Document]. https://doi.org/10.1139/cjss-2021-0033

Portes, R., Spinola, D., Ketterer, M.E., Egli, M., Lybrand, R.A., Fedenko, J., Biles, F., Trainor, T.P., Dere, A., D'Amore, D.V., 2024. Assessing decadal soil redistribution rates using 239+240Pu across diverse lithologies in Southeast Alaska. Soil Science Society of America Journal 88, 1659–1677. https://doi.org/10.1002/saj2.20732

Rhodes, E.J., 2011. Optically Stimulated Luminescence Dating of Sediments over the Past 200,000 Years. Annual Review of Earth and Planetary Sciences 39, 461–488. https://doi.org/10.1146/annurev-earth-040610-133425

Šamonil, P., Daněk, P., Schaetzl, R.J., Tejnecký, V., Drábek, O., 2018. Converse pathways of soil evolution caused by tree uprooting: A synthesis from three regions with varying soil formation processes. CATENA 161, 122–136. https://doi.org/10.1016/j.catena.2017.09.032

Šamonil, P., Daněk, P., Schaetzl, R.J., Vašíčková, I., Valtera, M., 2015. Soil mixing and genesis as affected by tree uprooting in three temperate forests. European Journal of Soil Science 66, 589–603. https://doi.org/10.1111/ejss.12245

Šamonil, P., Egli, M., Steinert, T., Norton, K., Abiven, S., Daněk, P., Hort, L., Brandová, D., Christl, M., Tikhomirov, D., 2020. Soil denudation rates in an old-growth mountain temperate forest driven by tree uprooting dynamics, Central Europe. Land Degradation & Development 31, 222–239. https://doi.org/10.1002/ldr.3443

Šamonil, P., Král, K., Hort, L., 2010. The role of tree uprooting in soil formation: A critical literature review. Geoderma 157, 65–79. https://doi.org/10.1016/j.geoderma.2010.03.018

Šamonil, P., Schaetzl, R.J., Valtera, M., Goliáš, V., Baldrian, P., Vašíčková, I., Adam, D., Janík, D., Hort, L., 2013. Crossdating of disturbances by tree uprooting: Can treethrow microtopography persist for 6000 years? Forest Ecology and Management 307, 123–135. https://doi.org/10.1016/j.foreco.2013.06.045

Šamonil, P., Valtera, M., Schaetzl, R.J., Adam, D., Vašíčková, I., Daněk, P., Janík, D., Tejnecký, V., 2016. Impacts of old, comparatively stable, treethrow microtopography on soils and forest dynamics in the northern hardwoods of Michigan, USA. CATENA 140, 55–65. https://doi.org/10.1016/j.catena.2016.01.006

Sanderson, D.C.W., Murphy, S., 2010. Using simple portable OSL measurements and laboratory characterisation to help understand complex and heterogeneous sediment sequences for luminescence dating. Quaternary Geochronology 5, 299–305. https://doi.org/10.1016/j.quageo.2009.02.001

Sauer, D., Sponagel, H., Sommer, M., Giani, L., Jahn, R., Stahr, K., 2007. Podzol: Soil of the Year 2007. A review on its genesis, occurrence, and functions. Journal of Plant Nutrition and Soil Science 170, 581–597. https://doi.org/10.1002/jpln.200700135

Schaetzl, R., Johnson, Donald, Burns, Scott, Small, T.W., 1989. Tree uprooting: review of terminology, process, and environmental implications. Canadian Journal of Forest Research.

Schaetzl, R.J., 1990. Effects of treethrow microtopography on the characteristics and genesis of Spodosols, Michigan, USA. CATENA 17, 111–126. https://doi.org/10.1016/0341-8162(90)90002-U

Schaetzl, R.J., 1986. Complete Soil Profile Inversion by Tree Uprooting. Physical Geography 7, 181–189. https://doi.org/10.1080/02723646.1986.10642290

Schaetzl, R.J., Burns, S.F., Small, T.W., Johnson, D.L., 1990. Tree Uprooting: Review of Types and Patterns of Soil Disturbance. Physical Geography 11, 277–291. https://doi.org/10.1080/02723646.1990.10642407

Schaetzl, R.J., Enander, H., Luehmann, M.D., Lusch, D.P., Fish, C., Bigsby, M., Steigmeyer, M., Guasco, J., Forgacs, C., Pollyea, A., 2013. Mapping the physiography of Michigan with GIS. Physical Geography 34, 2–39. https://doi.org/10.1080/02723646.2013.778531

Schaetzl, R.J., Follmer, L.R., 1990. Longevity of treethrow microtopography: implications for mass wasting. Geomorphology 3, 113–123. https://doi.org/10.1016/0169-555X(90)90040-W

Schaetzl, R.J., Kasmerchak, C., Samonil, P., Baish, C., Hadden, M., Rothstein, D., 2020. Acidification and weathering associated with deep tongues in sandy Spodosols, Michigan, USA. Geoderma Regional 23, e00332. https://doi.org/10.1016/j.geodrs.2020.e00332

Schaetzl, R.J., Loope, W.L., 2008. Evidence for an eolian origin for the silt-enriched soil mantles on the glaciated uplands of eastern Upper Michigan, USA. Geomorphology 100, 285–295. https://doi.org/10.1016/j.geomorph.2008.01.002

Schaetzl, R.J., Luehmann, M.D., Rothstein, D., 2015. Pulses of Podzolization: The Relative Importance of Spring Snowmelt, Summer Storms, and Fall Rains on Spodosol Development. Soil Science Society of America Journal 79, 117–131. https://doi.org/10.2136/sssaj2014.06.0239

Schimmack, W., Auerswald, K., Bunzl, K., 2001. Can 239+240Pu replace 137Cs as an erosion tracer in agricultural landscapes contaminated with Chernobyl fallout? Journal of Environmental Radioactivity, 53(1), 41-57. https://doi.org/10.1016/S0265-931X(00)00117-X

Shaler, N.S., 1891. Nature and Man in America. C. Scribner's sons.

Siame, L.L., Angelier, J., Chen, R.-F., Godard, V., Derrieux, F., Bourlès, D.L., Braucher, R., Chang, K.-J., Chu, H.-T., Lee, J.-C., 2011. Erosion rates in an active orogen (NE-Taiwan): A confrontation of cosmogenic measurements with river suspended loads. Quaternary Geochronology 6, 246–260. https://doi.org/10.1016/j.quageo.2010.11.003

Small, T.W., 1997. The Goodlett-Denny mound: a glimpse at 45 years of Pennsylvania treethrow mound evolution with implications for mass wasting. Geomorphology 18, 305–313. https://doi.org/10.1016/S0169-555X(96)00039-6

Spasić, M., Vacek, O., Vejvodová, K., Borůvka, L., Tejnecký, V., Drábek, O., 2024. Profile Development and Soil Properties of Three Forest Reclamations of Different Ages in Sokolov Mining Basin, Czech Republic. Forests 15, 650. https://doi.org/10.3390/f15040650

Stang, D.M., Rhodes, E.J., Heimsath, A.M., 2012. Assessing soil mixing processes and rates using a portable OSL-IRSL reader: Preliminary determinations. Quaternary Geochronology, 13th International Conference on Luminescence and Electron Spin Resonance Dating - LED 2011 Dedicated to J. Prescott and G. Berger 10, 314–319. https://doi.org/10.1016/j.quageo.2012.04.021

Tejnecký, V., Šamonil, P., Matys Grygar, T., Vašát, R., Ash, C., Drahota, P., Šebek, O., Němeček, K., Drábek, O., 2015. Transformation of iron forms during pedogenesis after tree uprooting in a natural beech-dominated forest. CATENA 132, 12–20. https://doi.org/10.1016/j.catena.2015.04.005

Wallinga, J., 2002. Optically stimulated luminescence dating of fluvial deposits: A review. Boreas 31, 303–322. https://doi.org/10.1111/j.1502-3885.2002.tb01076.x

Wittmann, H., von Blanckenburg, F., Bouchez, J., Dannhaus, N., Naumann, R., Christl, M., Gaillardet, J., 2012. The dependence of meteoric 10Be concentrations on particle size in

Amazon River bed sediment and the extraction of reactive 10Be/9Be ratios. Chemical Geology 318–319, 126–138. https://doi.org/10.1016/j.chemgeo.2012.04.031

Xu, Y., Qiao, J., Pan, S., Hou, X., Roos, P., Cao, L., 2015. Plutonium as a tracer for soil erosion assessment in northeast China. Science of The Total Environment 511, 176–185. https://doi.org/10.1016/j.scitotenv.2014.12.006

Yost, J.L., Hartemink, A.E., 2019. Soil organic carbon in sandy soils: A review, in: Advances in Agronomy. Academic Press, pp. 217–310. https://doi.org/10.1016/bs.agron.2019.07.004

Zollinger, B., Alewell, C., Kneisel, C., Brandová, D., Petrillo, M., Plötze, M., Christl, M., Egli, M., 2017. Soil formation and weathering in a permafrost environment of the Swiss Alps: a multi-parameter and non-steady-state approach. Earth Surface Processes and Landforms 42, 814–835. https://doi.org/10.1002/esp.4040

Zollinger, B., Alewell, C., Kneisel, C., Meusburger, K., Brandová, D., Kubik, P., Schaller, M., Ketterer, M., Egli, M., 2015. The effect of permafrost on time-split soil erosion using radionuclides (137Cs, 239 + 240Pu, meteoric 10Be) and stable isotopes (δ13C) in the eastern Swiss Alps. J Soils Sediments 15, 1400–1419. https://doi.org/10.1007/s11368-014-0881-9

Personal Declaration

Personal declaration: I hereby declare that the submitted thesis is the result of my own, independent work. All external sources are explicitly acknowledged in the thesis.

I acknowledge that ChatGPT (OpenAI) was used to improve the grammar and syntax in this text, and the code in RStudio.

Waldkirch, April 24, 2026

Annika Spaar